Regional-Scale Flows in Mountainous Terrain. Part I: A Numerical and Observational Comparison

JAMES E. BOSSERT

Earth and Environmental Sciences Division, Los Alamos National Laboratory, Los Alamos, New Mexico

WILLIAM R. COTTON

Department of Atmospheric Science, Colorado State University, Fort Collins, Colorado

(Manuscript received 24 May 1993, in final form 26 November 1993)

ABSTRACT

This study uses observed data and a numerical simulation to examine the generation of thermally driven flows across the Colorado mountain barrier on meso-β to meso-α scales. The observations were collected from remote surface observing systems at exposed mountaintop locations throughout the state of Colorado, over the summers of 1984–88, as part of the Rocky Mountain Peaks Experiment (ROMPEX). The data show the development of a recurrent circulation system across the Colorado mountain barrier, operating on a diurnal timescale. From the observations, the basic structure of the flow system appears as a daytime inflow toward the highest terrain, and a nocturnal outflow away from it. However, when examined in detail, the flow system exhibits more unusual behavior, especially west of the barrier crest. Here, winds in the early evening are occasionally observed to onset abruptly from an easterly direction, generally counter to the upper-level winds. Observations from ROMPEX for 26 August 1985 are used to provide comparison data for a numerical simulation with the Regional Atmospheric Modeling System (RAMS). This three-dimensional case study experiment is initialized with data from the National Meteorological Center and incorporates two-way interactive grid nesting.

From the observed data and case study simulation, four distinct phases of the regional-scale circulation system have been identified. In the development phase, a deep mountain–plains solenoid is generated through terrain heating along the Front Range. This circulation system transforms in the late afternoon transition phase into a westward-propagating density current (WPDC). The third phase, called the "density-current propagation phase," occurs as the WPDC moves westward across the mountains, leaving in its wake strong southeasterly flow at the mountaintop level. This current appears to be the cause of the peculiar easterly component winds found in the ROMPEX mountaintop observations along the western slope. In the final late-night adjustment phase, the WPDC dissipates near the western edge of the Colorado mountains and a steady southerly flow evolves over the high mountain terrain. This southerly flow is the steady response to the differential heating that develops between the low-lying plains and the intermountain region.

1. Introduction

For more than a century, scientists have studied the pervasive wind circulations that occur in regions of sloping terrain. Early observations showed that air motion down the slopes was a dependable phenomenon at night, while a general up-the-slope wind was the rule by day. Despite the apparent simplicity of this diurnal flow regime, a working theoretical explanation eluded early meteorologists until the development of the Bjerknes circulation theorem (Jeffreys 1922). These early theories were greatly expanded upon in later years (Wagner 1938; Defant 1951) to include more complicated and realistic forcing mechanisms over the slopes and to include the circulations within mountain valleys.

While much of the early research attention was focused upon thermally driven flows along small-scale slopes and within mountain valleys (micro-α to meso-β scales), more recent observations have shown that terrain-induced flows can also be found on meso-β to meso-α scales (20–2000 km). For example, in South Africa, Tyson and Preston-Whyte (1972) described a diurnally oscillating circulation system that evolved in winter between the Natal coast and the Drakensburg Plateau, a horizontal distance of 200 km. These authors called this circulation system the "mountain–plain" wind, to distinguish it from smaller-scale mountain–valley winds. In the United States, similar thermally forced circulation systems with horizontal scales over 100 km have been found in Washington State (Staley 1957; Doran and Zhong 1994) and along the Colorado Front Range in summer (Toth and Johnson 1985).

Corresponding author address: Dr. James E. Bossert, Earth and Environmental Sciences Division, Mail Stop D401, Los Alamos National Laboratory, Los Alamos, NM 87545.

Given that these flows can cover a large topographic region in scale, they are regarded here as "regional-scale" flow systems, as a convenient way of separating them from smaller-scale mountain–valley flows, or synoptic-scale thermally forced wind systems, which can encompass large plateau areas (e.g., Tang and Reiter 1984).

In the available literature through the 1970s, observational evidence of regional-scale flows was very limited (see Barry 1992; Atkinson 1981). However, recent measurement programs and numerical studies have demonstrated the prominent nature of these wind systems. For example, special surface-based observing networks have allowed several researchers to observe the diurnal evolution of the summertime mountain–plain circulation along the Front Range of the Rocky Mountains (Banta and Cotton 1981; Toth and Johnson 1985). In the vertical plane, this regional-scale circulation forms a pressure–density solenoid (Holton 1979) consisting of low-level upslope flow, strong upward motion near the barrier crest, and a return circulation away from the barrier above the crest. This solenoid has been shown to be an important factor in the development of convective storms, which can propagate eastward and evolve into large mesoscale convective complexes over the Great Plains (Tripoli and Cotton 1989a,b; Tremback 1990). These convective complexes bring a high percentage of the total summer rainfall to the Midwest. In Washington State, similar diurnally forced regional-scale flow systems have been associated with an increase in nocturnal precipitation over the Puget Sound region (Mass 1982).

Evidence of a thermally driven, regional-scale flow regime in a layer above the mountain–valley circulations, similar to that described by Tyson and Preston-Whyte (1972), was also discovered over the extremely complex terrain of the western slope of the Rocky Mountains within Colorado (Whiteman 1980; Bader et al. 1987). The principal characteristics of this western slope circulation system have recently been obtained through an observational program known as the Rocky Mountain Peaks Experiment (ROMPEX) that was conducted over the summers of 1984–88 and is described in several papers (Reiter et al. 1987; Bossert and Reiter 1987; Sheaffer and Reiter 1987; Bossert et al. 1989; Bossert 1990).

In this paper, we provide a detailed, three-dimensional investigation of thermally induced meso-β- to meso-α-scale wind systems across the Colorado Rocky Mountain barrier, based upon the ROMPEX observations. The purpose of the study is to examine the structure of regional-scale circulations over the Colorado mountains and the primary mechanisms forcing their diurnal evolution. Through these efforts we hope to provide insight into the complex dynamics occurring on a multitude of scales that ultimately produce the hierarchical system of thermally forced flows found over complex terrain.

In the following sections we first examine observational data of regional-scale flows (section 2). Next, we examine observations for the chosen case day, around which the numerical study was formulated (section 3). In section 4, we describe the mesoscale model and the specific configuration used for this study. Results from the case study simulation and a comparison with ROMPEX observations are presented in section 5, and in section 6 a conceptual model of the regional-scale flow evolution across the Colorado Rocky Mountain barrier is discussed. Conclusions from this study are presented in section 7. In a companion paper, Bossert and Cotton (1994), we present results from idealized experiments that isolate the influence of surface heating, topographic configuration, ambient wind speed and shear, stratification, and variable ground wetness on the evolution of regional-scale flows.

2. Observational development

One of the goals of the ROMPEX experiments was to monitor the wind field at mountaintop during the summer season and analyze the departure of these winds from the overlying synoptic-scale flow in high-altitude complex terrain locations. This was accomplished with surface stations placed at remote mountaintop sites and equipped with instrumentation to record basic meteorological parameters.

Results from the ROMPEX mountaintop measurement program revealed the existence of a recurrent flow phenomenon across the mountain barrier. In its most basic form, this wind system consisted of a regional-scale (meso-β scale) flow varying between daytime winds toward, and nocturnal outflow away from, the highest mountains (see Fig. 2, Bossert et al. 1989). The diurnal nature of the flow regime points toward a thermally direct circulation system forced by differential heating of the elevated terrain. This circulation system was particularly pronounced across a region of north-central Colorado encompassing the 1985 mountaintop stations of Mount Werner, Buffalo Pass, Flat Tops, Vail Mountain, Elk Mountain, Rocky Mountain Park, Mines Peak, Squaw Mountain, and Rollinsville (MW, BP, FT, VA, EK, RM, MI, SQ, and RO in Fig. 1). Also shown in Fig. 1 is a schematic of the "eastern" and "western" slopes, the "barrier crest," and the "intermountain region," all terms that are used extensively here to define the wind regime relative to the existing topography. The altitude and type of data collected at each of these stations was described in Reiter et al. (1987) and Bossert et al. (1989).

Of particular interest in the ROMPEX data was the periodic appearance of strong, nocturnal southeasterly winds at virtually all of the peaktop stations west of the barrier crest. An example of this is shown in the time series of Fig. 2 during a 7-day period of August 1984 for Mount Werner (MW) at the top of the Steamboat ski resort. The figure shows a shift in wind direction

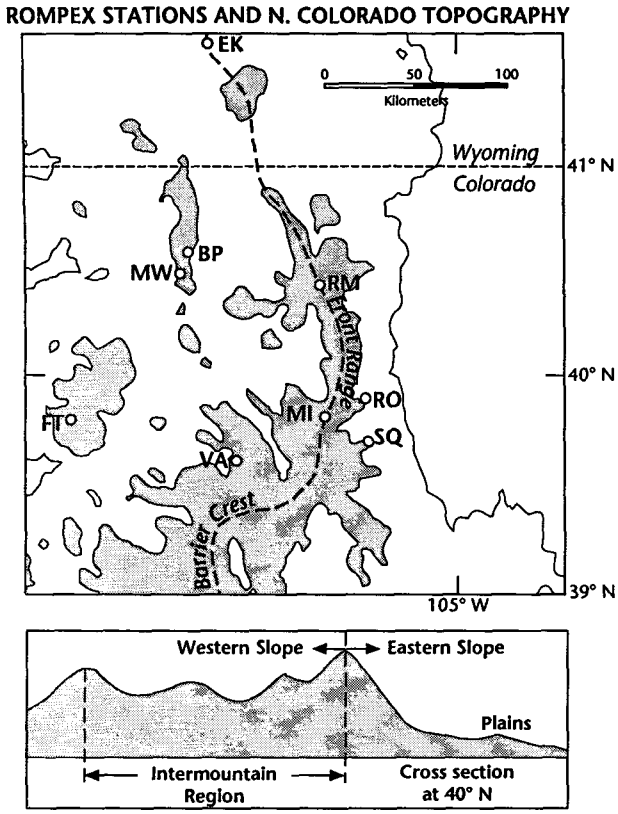

FIG. 1. Upper: geographic location of ROMPEX-85 stations and two-letter identifiers discussed in text. Topographic contours are 2000 and 3000 m MSL. Areas above 3000 m MSL are shaded. Lower: schematic of topography terms used in text.

each day from an afternoon northwest wind to much stronger southeasterly winds at night. Given the exposed mountaintop location of this station at the 70-kPa level, and prevailing ambient flow with a westerly component during this period, the systematic appearance of strong evening and nocturnal easterly component flow was very unusual. There also appeared to be a high correlation among the onset time of the easterly flow between MW and other mountaintop stations (Bossert and Reiter 1987). Nighttime soundings have shown the nocturnal southeasterly flow at MW to be shallow over the peaktops (~500 m) with a low-level jet structure within a distinct and highly stratified layer (Bossert et al. 1989).

Several processes that could produce the diurnal regional-scale inflow–outflow regime, and in particular, the abrupt evening wind reversal and sustained nocturnal easterly flow at stations west of the barrier crest were suggested by Bossert et al. (1989). The most obvious of these was strong summertime terrain heating and cooling. Less obvious was outflow from convective storms over the high terrain of Colorado, which were found to promote an earlier onset time of the southeasterly winds, as well as increase their strength (Bossert 1990). However, neither of these mechanisms could provide a complete picture, since the onset time of the southeasterly outflow at MW often occurred well before sunset and possessed characteristics much like a thunderstorm gust front. This would preclude terrain cooling as the primary forcing mechanism while strongly suggesting that deep convection over the high mountains was somehow forcing the observed outflow regime. The easterly winds, however, often occurred for 10–12-h periods on days with little or no moist convection, eliminating deep convection as the main contributor. Our incomplete knowledge of the processes involved in the generation of the regional-scale easterly component flow has lead to the present study, which attempts to simulate the complete mesoscale circulation that developed on a well-documented day in August 1985. Here, we address only the circulations that developed on a day with virtually no moist convective processes. It is left as a future project to further investigate the influence of strong convection upon wind patterns over high mountain terrain.

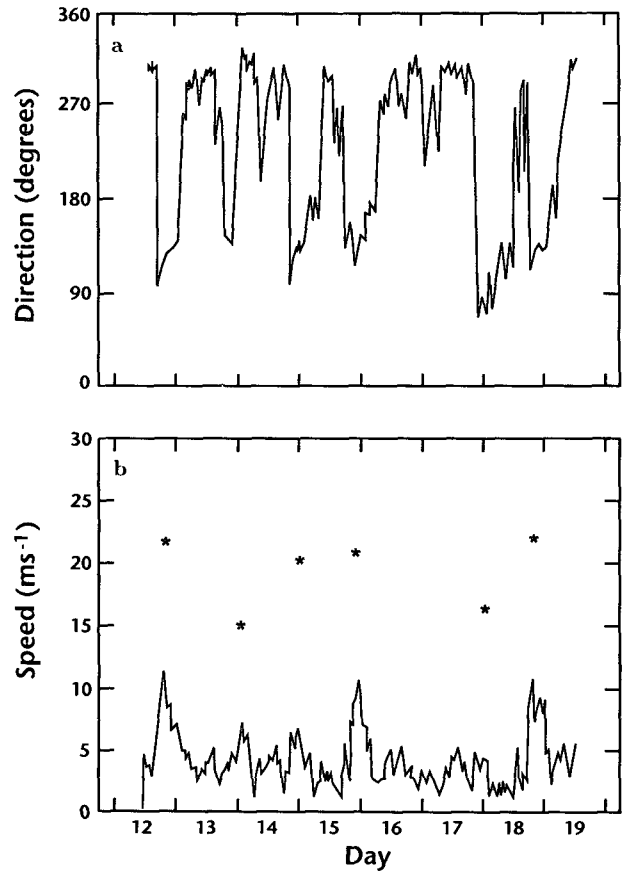

FIG. 2. (a) Wind direction and (b) wind speed for 30-min-averaged intervals for 12–19 August 1984. Asterisks in (b) denote maximum wind gust speeds.

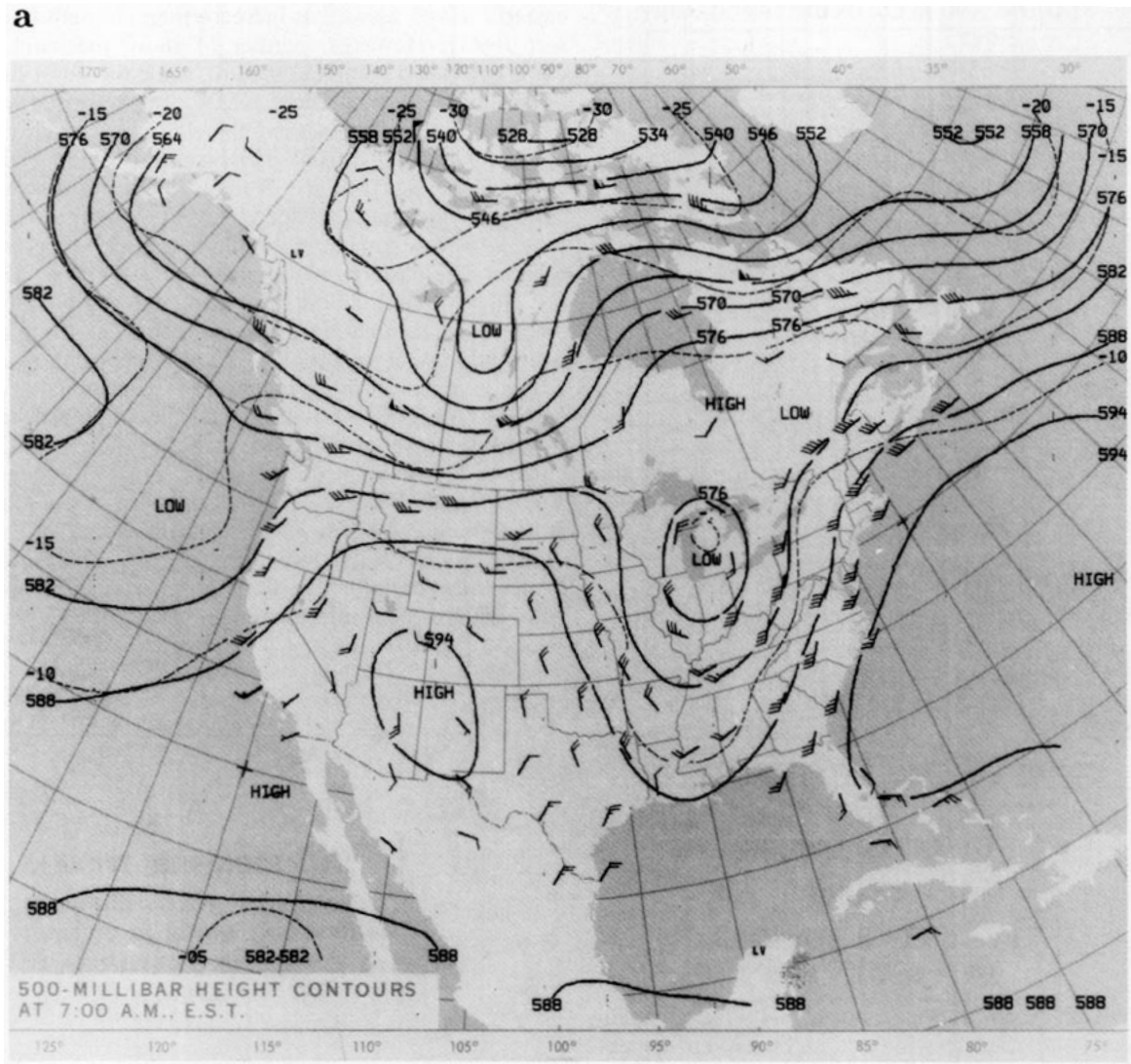

FIG. 3. Geopotential heights at 50 kPa for (a) 0500 LST (1200 UTC) 26 August 1985 and (b) 0500 LST (1200 UTC) 27 August 1985 (from Daily Weather Maps, National Oceanic and Atmospheric Administration, Department of Commerce).

3. Case study day: 26 August 1985

a. Large-scale observations

In an effort to further understand the development of the regional-scale circulation systems described previously, a case study day has been selected for initializing numerical simulations. The period chosen for study is 0500 LST (1200 UTC) 26 August to 0500 LST (1200 UTC) 27 August 1985. During this period, a broad ridge of high pressure at 50 kPa over the western United States (Fig. 3) produced very warm temperatures and low humidities over the Colorado Rocky Mountains. The prevailing dry conditions virtually eliminated thunderstorm effects, while weak synoptic pressure gradients allowed surface thermal forcing to develop a well-defined mesoscale flow response over the mountain region. At the surface (not shown), weak pressure gradients and generally light and variable winds occurred over the western United States in association with the upper-level ridge.

b. Regional-scale conditions

The vertical structure over Colorado on 26 August is given in Fig. 4 at 0500 LST (1200 UTC) for both Denver (DEN) and Grand Junction (GJT), and at GJT only for 1700 LST (0000 UTC 27 August), since no sounding was reported for DEN at that time. The potential temperature at 0500 LST (Fig. 4a) is very similar between the two stations through the entire depth of the sounding. A strong low-level inversion gives way near the surrounding mountain barrier height

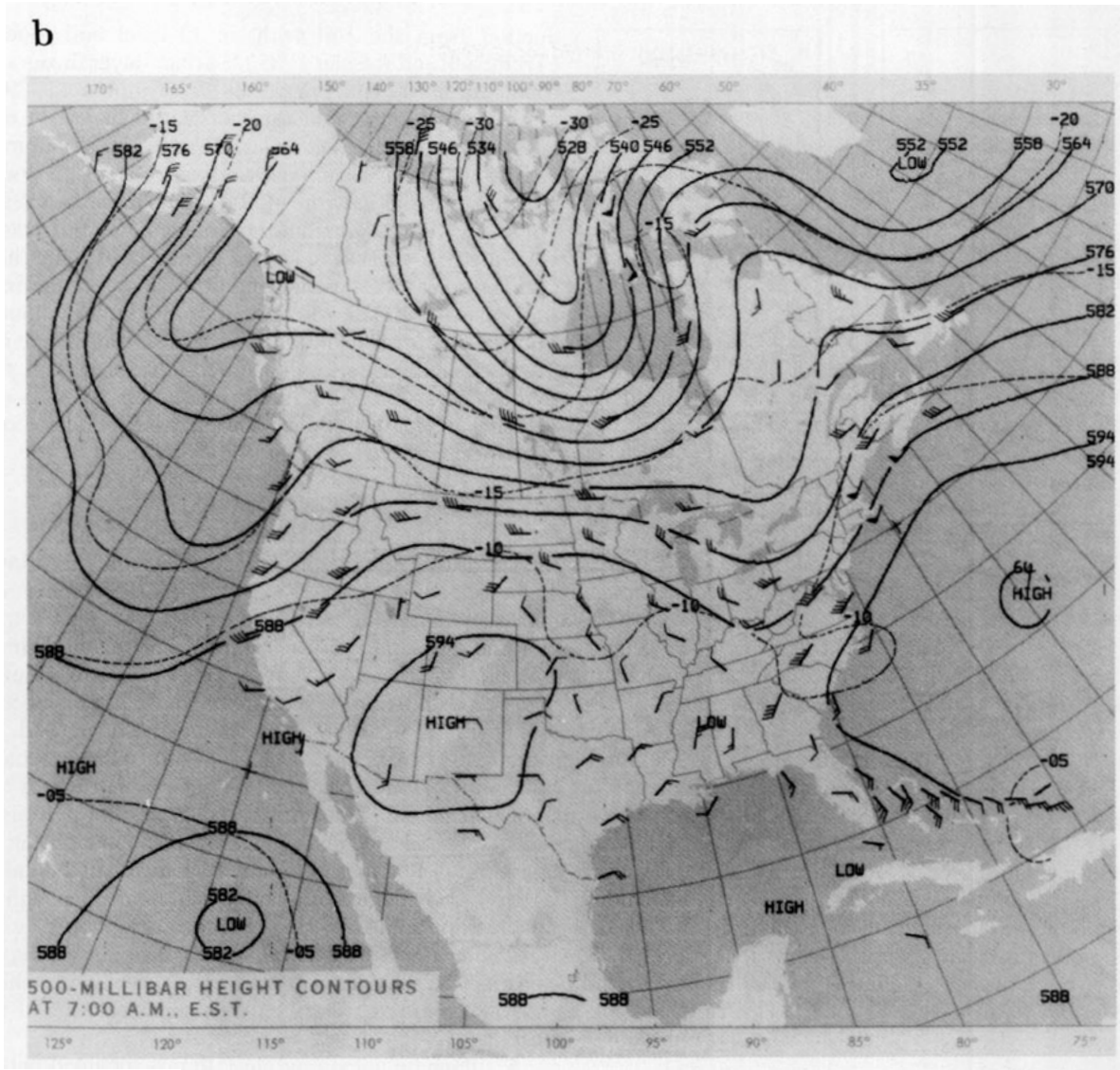

FIG. 3. (*Continued*)

(~3200 m MSL) to a weakly stable atmosphere that persists to 8000 m MSL at DEN. The unstable layer in the GJT sounding between 5000 and 6000 m MSL appears to be caused by an erroneous temperature reading at the 50-kPa level. Twelve hours later, the 1700 LST sounding at GJT shows the development of a mixed layer to 5200 m MSL, 3700 m above the surface. Above the surrounding mountain level (~3200 m MSL), conditions are largely unchanged from the morning sounding, indicative of fairly stagnant conditions that prevailed under the broad upper-level ridge.

The wind profiles at 0500 LST 26 August (Fig. 4b) are also very similar between DEN and GJT, with terrain-influenced wind systems apparent below 3200 m MSL at each station. Northwesterly flow occurs near the top of the low-level inversion in both soundings, which back toward a westerly direction in the upper troposphere. Wind speeds are very light, less than 10 m s^{-1} all the way to 9000 m MSL (~33 kPa). The winds become even weaker in the 1700 LST GJT sounding, with speeds less than 5 m s^{-1} up to 7600 m MSL. Wind direction at 1700 LST shifts from a northwest direction near the surface to southwesterly flow at 5000 m MSL.

A geographical depiction of averaged afternoon and late night winds for the various ROMPEX stations operating during the case study day was provided in Fig. 2 of Bossert et al. (1989), which demonstrated the distinct inflow–outflow signature of the regional-scale flow across the Colorado mountain barrier. Additional analyses of ROMPEX data for this case day are deferred until section 5d, where comparisons are made between the case day simulation and ground-based ROMPEX observations.

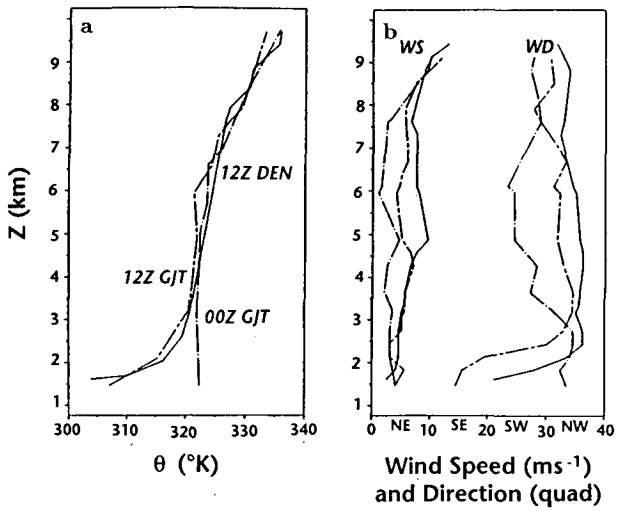

FIG. 4. Vertical profiles of (a) potential temperature θ and (b) wind speed and wind direction for Denver (DEN; solid line) and Grand Junction (GJT; dashed line) at 0500 LST (1200 UTC) 26 August 1985 and for GJT (dash–dot line) at 1700 LST (0000 UTC) 27 August 1985.

With the aid of these observational analyses, we were able to assess the meteorological conditions at mountaintop on this case day, which shows evidence of a distinct diurnally varying wind regime whose phase reverses across the mountain barrier. Still, the ROMPEX data are very limited in their temporal and spatial resolution and at only 3 m AGL. Thus, in the following section we describe a numerical simulation designed to provide an additional analysis tool for understanding the regional-scale circulations that evolved across the Colorado mountain barrier on 26 August 1985.

4. Simulation development

a. Model description

The mesoscale model chosen for the study is the Regional Atmospheric Modeling System (RAMS) developed at Colorado State University. RAMS is a highly flexible system and has been used to simulate a wide variety of mesoscale phenomena. This terrain-following, primitive equation model has most recently been described in Pielke et al. (1992) and in the extensive references included therein. The RAMS version in the present study uses a nonhydrostatic model framework with a terrain-following vertical coordinate [$\sigma_z = z_T(z - z_G)/(z_T - z_G)$; where z_T is the height of the model top and z_G is the height of the terrain, and z is the height above the terrain]. At the lower boundary, surface-layer temperature and moisture fluxes are determined from the surface energy balance, which incorporates both longwave and shortwave radiative fluxes, latent and sensible heat fluxes, and heat and moisture conduction from the soil with an 11-level soil model (Tremback and Kessler 1985). Surface-layer fluxes are based upon the parameterization of Louis (1979), which uses Monin–Obukhov similarity theory to describe the constant flux layer. Turbulence is parameterized using an eddy viscosity based upon the local deformation field, with additional enhancements including a Richardson number dependence. The parameterization of shortwave and longwave radiation (Chen and Cotton 1983) considers absorption, scattering, transmission, and emission from both clear and cloudy atmospheric layers. The simulation described herein includes water vapor for its important effect upon the disposition of the radiative fluxes; otherwise, it is essentially a passive tracer within the model with no condensation allowed to occur.

b. Grid structure

A two-way interactive grid nesting scheme following Clark and Farley (1984) is employed in the simulation. Grid nesting allows the focusing of higher spatial and temporal resolution on desired regions within the model domain with greater computational efficiency. With two-way interaction, nested grids receive boundary information from the next coarser grid. In turn, results from each nested grid are averaged back to the next coarser grid, which greatly influences the model solutions. In this study, grid nesting permits a high-resolution simulation over the complex terrain of the central Rocky Mountains while still maintaining coarser grids that encompass a region large enough to resolve important synoptic-scale and regional-scale information. In addition, higher-resolution topography data can be incorporated into each nested grid, which provides an increasingly realistic representation of the terrain forcing.

A silhouette averaging algorithm is included within the RAMS code to enhance the topographic representation by preserving the actual heights of mountain barriers. The scheme provides for any permutation between conventional and full silhouette averaging by use of a weighting factor. Any desired amount of topography smoothing may also be accomplished.

To obtain the topography silhouette, the user defines a topography grid at lower spatial resolution than the actual model grid and generally much lower resolution than the topography dataset (5-min data used in this study). Initially, the scheme finds the height of the silhouette as viewed from the east–west and north–south by taking the maximum heights from all of the data points in each direction of the topography grid cell. These two directional height profiles are then averaged to obtain a mean height, which constitutes the silhouette averaged height of a topography grid cell. Conventional averaging is also done to obtain a mean height for each topography grid cell. When this procedure is completed for all of the topography grid cells

that encompass the model grid domain, the topography grid heights are then multiplied by a user-defined weighting factor that determines the degree of the topography silhouette that is retained (e.g., 0 for traditional mean topography profile up to 1.0 for full silhouette). This factor is generally increased for higher-resolution grids. The topography grid data is then interpolated to the model grid. For the present investigation, this silhouette averaging technique was applied to improve the representation of the high mountains and their slopes over Colorado.

Interpolation of the topography grid data is also used for smoothing the topography data. For example, since the shortest resolvable wavelength in the model is $2\Delta x$, specification of a coarser topography grid cell at twice the model grid cell size means that no modes shorter than $4\Delta x$ will exist when the topography grid is interpolated onto the model grid.

The case day simulation is three-dimensional and uses a latitude–longitude grid configuration with three grids. The areal coverage of the three grids is shown in Fig. 5a, which also shows the topography heights and initial wind vectors on grid 1 plotted at every grid point. The coarsest grid has 1.0° resolution in latitude and 1.3° resolution in longitude. This grid specification provides an approximately equal horizontal grid cell dimension of approximately 111 km at 40°N, which is the latitude of primary interest. The next finer grid incorporates a 4:1 nesting ratio, which gives an approximate 28-km horizontal resolution at 40°N. The third and highest resolution grid is again at a 4:1 nesting ratio from the second grid, providing an approximate grid spacing of 7 km. The three grids consist of 30, 42, and 58 zonal grid cells and 30, 34, and 54 meridional grid cells, respectively. The topographic representation over the third grid (see Fig. 7) resolves the major mountain ridges and valleys of north-central Colorado, the primary region of interest. A stretched vertical grid spacing is employed, which varies the vertical resolution from 100 m near the surface to a constant value of 500 m at 3.5 km and above. All model grids have 42 vertical levels, with the top at 17.15 km AGL. The upper boundary consists of a rigid lid, and radiative lateral boundary conditions are employed following Klemp and Wilhelmson (1978a,b).

c. *Model initialization*

The model simulation is initialized with data from the National Meteorological Center's (NMC) 2.5° gridded pressure-level data, which is supplemented with standard rawinsonde and surface observations. This data is blended together by means of vertical interpolation and an objective analysis (Barnes 1973) onto an isentropic grid at specified levels, with a scheme developed in Tremback (1990). The gridded isentropic data are then interpolated onto the coarse model grid, after which the nested grids are initialized by interpolation from the coarse grid. For this case study, the model is initialized at 1700 LST 25 August 1985 (0000 UTC 26 August) and run for a 36-h period. The five outermost lateral boundary points are nudged with the technique described in Davies and Turner (1977), toward the objectively analyzed gridded data for 0500 LST (1200 UTC 26 August) for the initial 12-h period and toward subsequent NMC analyses for the 24- and 36-h periods of the run. During the 12-h period from 1700 LST 25 August to 0500 LST 26 August 1985, the model adjusts to the imposed large-scale fields. In addition, simulated radiative cooling over the complex model terrain during this nocturnal period produces a more realistic low-level stratification than is possible from standard initialization techniques.

5. Simulation results

Of interest for this case study is the 24-h diurnal period beginning at 0500 LST 26 August 1985. Since the initial state of the simulation was at 1700 LST 25 August 1985, the beginning of the case study period is in actuality a 12-h prediction. The simulated fields are shown in Fig. 5 and can be compared with the observed synoptic-scale data presented in Fig. 3. At $z = 5.65$ km above the terrain surface (Fig. 5a), a well-defined upper-level ridge is centered over the Four Corners region of the southwestern United States. The location of this feature, as well as the short wave at the United States–Canada border, and the strong northerly flow over the midwestern United States are all in reasonable agreement with the 50-kPa height field shown in Fig. 3a for the same time. Near the surface, westerly flow is simulated over the central Rocky Mountains (Fig. 5b), with a lee trough in evidence along the Front Range, which also appears in the observed surface analysis (not shown). The near-surface (~50 m) potential temperature field over the coarse grid domain (Fig. 5c) shows that the warmest air resides over the elevated plateau of the intermountain west. The mixing ratio at approximately 50 m (Fig. 5d) reveals that conditions are very dry over the interior of the western United States, including the Colorado mountains.

a. *Simulated daytime circulations*

The westerly component low-level flow over the north-central Colorado mountain region, shown in Fig. 5b for 0500 LST, persists into the morning hours. Figure 6 is a west–east cross section of grid 3 from the Flat Tops to the Front Range at 40°N and shows the presence of a mountain wave disturbance and strong downslope flow at 0900 LST (Fig. 6a), generated by stable northwesterly flow above the barrier crest (Fig. 6b). This mountain wave is gradually dissipated from below, however, by easterly upslope flow within the shallow, developing boundary layer noticeable by this time along the eastern slope (Fig. 6b).

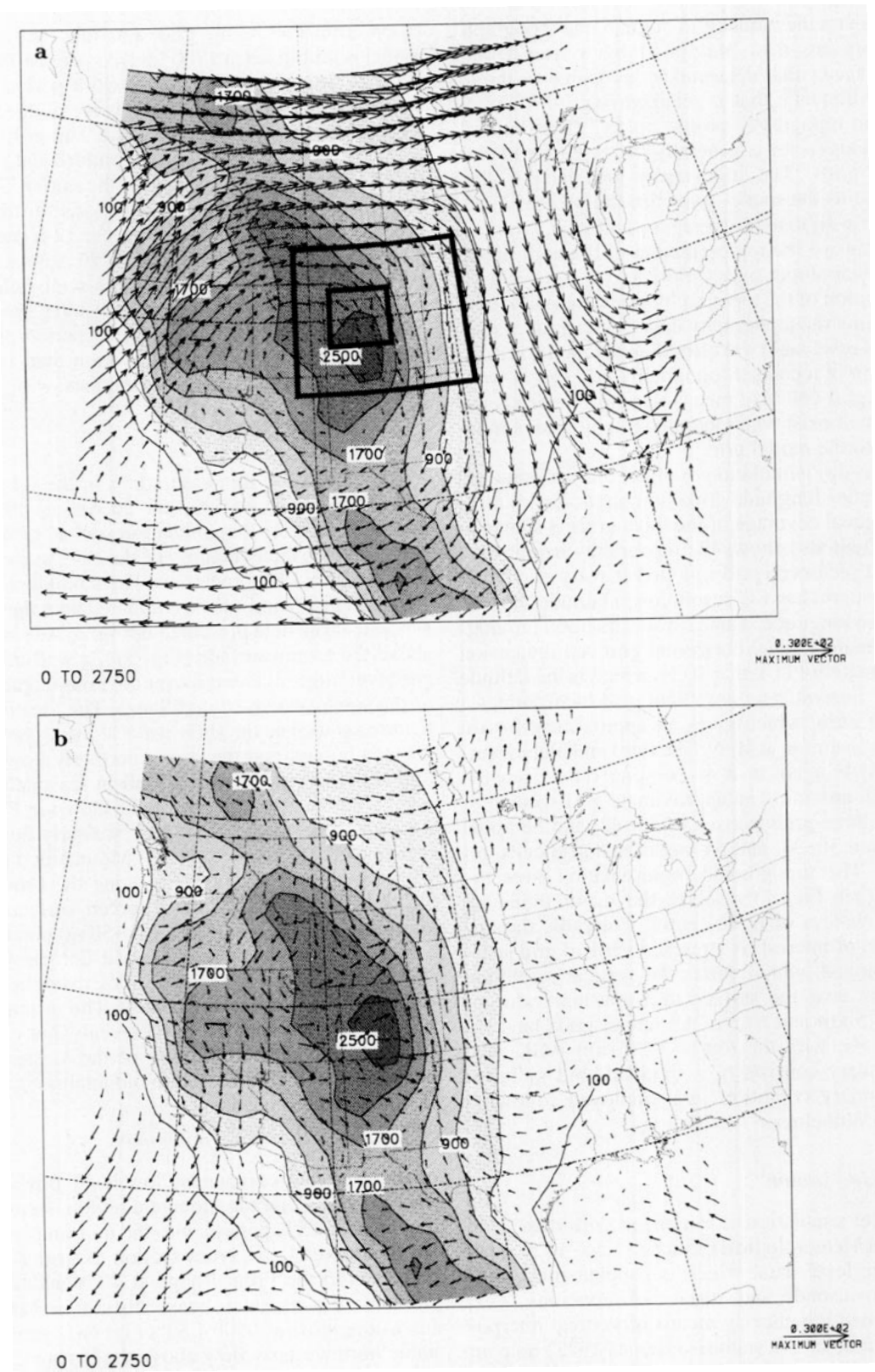

FIG. 5. Wind vectors at every grid point and topography (contours every 400 m) at (a) 5.65 km AGL, and (b) 0.05 km AGL, (c) potential temperature at 0.05 km AGL (contour interval 3°C), and (d) mixing ratio at 0.05 km AGL (contour interval 1.0 g kg^{-1}) on grid 1 at 0500 LST (1200 UTC) 26 August 1985. Bold solid lines in (a) denote the geographic location of grids 2 and 3.

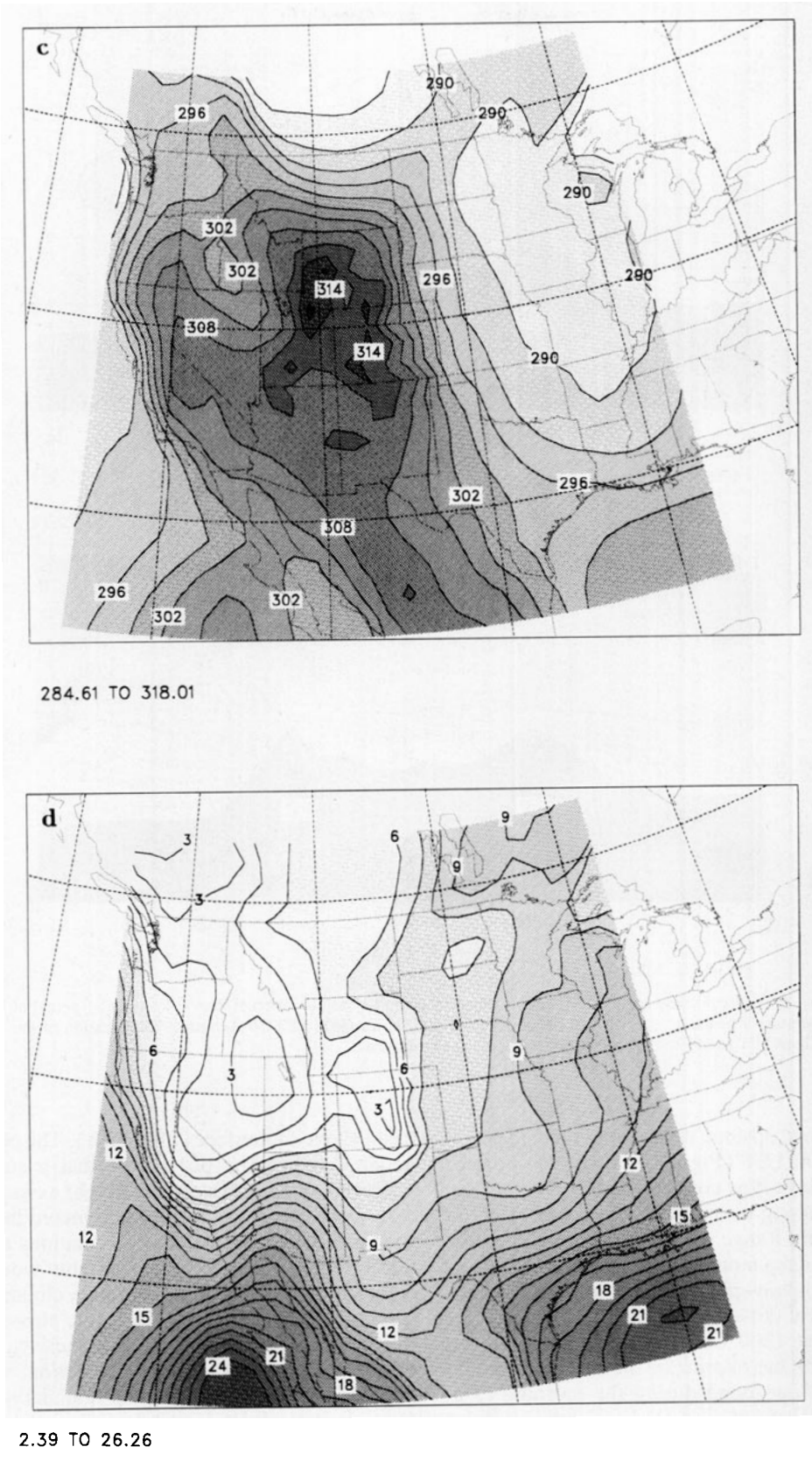

FIG. 5. (*Continued*)

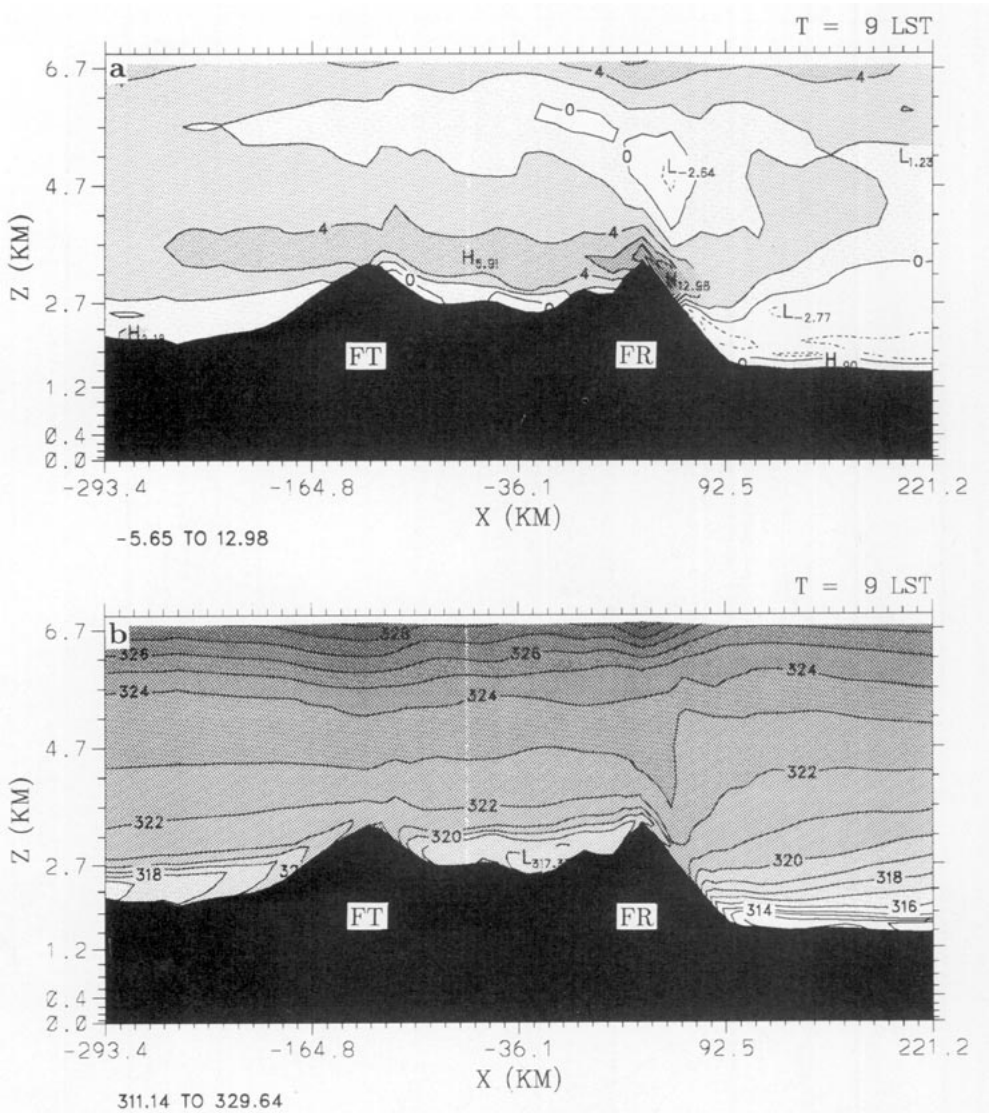

FIG. 6. Vertical cross sections of (a) u-component wind (contour interval 2 m s^{-1}) and (b) potential temperature θ (contour interval 1.0°C) on grid 3 at 40.0°N for 0900 LST 26 August 1985. Location of the Flat Tops (FT) and Front Range (FR) indicated for reference.

The eastern slope upslope circulation intensifies dramatically by 1300 LST (Fig. 7) with further surface heating. The upslope flow converges at the barrier crest and is prevalent along the entire north–south extent of the Colorado Front Range. This circulation is the low-level branch of a deep mountain–plains circulation, the Front Range mountain–plains circulation (FRMC), as shown in a vertical cross section of the model domain through 40.0°N at 1300 LST (Fig. 8). The vigorous upslope circulation has eliminated the shallow westerly mountain wave flow found during the morning (Fig. 8a). Upslope flow from a westerly direction is also evident over the western slope of the Flat Tops Range. Weak northwesterly winds, characteristic of the upper-level flow, are present over much of the intermountain basin above the surface (Figs. 8a,b). The potential temperature field (Fig. 8c) shows that a superadiabatic lapse rate that decreases with height exists in the planetary boundary layer, while deep mixed layers exist in the vicinity of the ascending circulations at the mountain crests. These ascending currents would have resulted in the formation of cumulus clouds had supersaturation been allowed. However, atmospheric conditions and a lack of moisture were unfavorable for the development of deep moist convection, which could have influenced the developing boundary-layer flows. Over the rest of the domain boundary layer depths are on the order of 1.0–1.5 km. Due to the deep mixing in the ascending branch of each solenoid, a region of high baroclinicity begins to develop in the atmosphere above

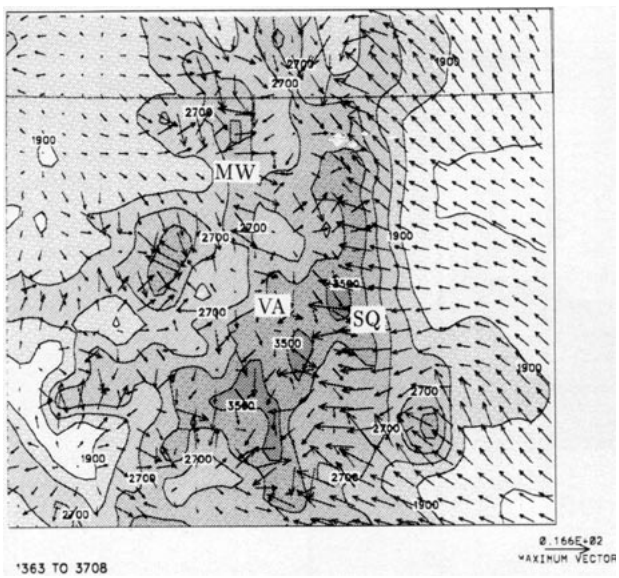

FIG. 7. Wind vectors plotted at every other grid point and topography (contour interval 400 m) on grid 3 at 0.05 km above the surface for 1300 LST 26 August 1985. Location of the Mount Werner (MW), Vail Mountain (VA), and Squaw Mountain (SQ) ROMPEX stations indicated for reference.

each principal slope of the central Rocky Mountain barrier.

b. *Simulated transition phase*

In late afternoon, the surface sensible heat flux begins a steep decline, eventually reaching zero net heating between 1700 and 1800 LST, more than 1 h before sunset (see Fig. 2, Bossert and Cotton 1994). Cooling of the surface begins at this point in time, generating stable air near the surface and decoupling the surface from the deep mixed layer above. This scenario begins the "transition" phase of the diurnal circulation, since now those circulations generated through surface heating, such as the FRMC, will become detached from their source. The fate of these mesoscale circulations produced by the diurnal heating cycle is of particular interest to this study and is described in the following section.

A vertical cross section (Fig. 9) will serve to illustrate the structure of the wind and temperature fields associated with the regional-scale wind regime that has evolved by 1700 LST (0000 UTC 27 August). This time is approximately 90 min prior to simulated sunset, and marks the incipient transition phase of the heating-generated circulations. The potential temperature field (Fig. 9a) shows that a significant horizontal temperature gradient exists within the FRMC, just west of the Front Range crest. This baroclinic zone separates the deep, very warm boundary layer over the intermountain region in which weak, primarily westerly wind prevails, from the relatively shallow, cool boundary-layer air mass located along the eastern slope of the Front Range, where stronger easterly component flow exists (Fig. 9b). A more diffuse thermal gradient with similar characteristics is also present along the eastern slope of the Flat Tops Range and separates the far western slope and intermountain air masses.

An interesting result from this simulation involves the late afternoon–early evening westward advection of potentially cooler air across the crest of the barrier. This westward advection is documented in Fig. 10, which shows the potential temperature field at about 50 m superimposed with the vector winds for the period 1700–2000 LST. Visible in these plots is a clearly delineated "front" at 1700 LST (Fig. 10a) along the length of the mountain barrier between the air masses over the eastern and western slopes of the Front Range. Also apparent are stronger easterly winds behind the front, continuously reinforcing the cold air at the front. This cold advection advances the front farther west (Fig. 10b) over the next hour (1800 LST), where it undercuts the turbulent, very homogeneous air mass over the intermountain region of Colorado. The onset of strong surface cooling by 1900 LST (Fig. 10c) begins to produce some inhomogeneity in the intermountain air mass at this 50-m level; however, the thermal gradient along the advancing front remains quite strong. At 2000 LST, the front continues its advance westward across the high mountain topography (Fig. 10d) and further intensifies, particularly within the central portion of the simulation domain.

Over this 3-h period the low-level front is simulated to propagate 50–75 km in a northwestward direction, depending upon the latitude, with the farthest propagation distance in the southern portion of the domain. This yields a propagation speed of 5–7 m s^{-1}. Many of the characteristics of the propagating front are similar to those associated with thunderstorm outflows or density currents, as described by Charba (1974). These include the well-defined wind speed and temperature gradients in the frontal zone, the higher wind speeds behind the front, and the distinctive appearance of the colder air mass. Given these features, we can compare the simulated frontal speed with that from Cotton and Anthes (1989) for a propagating density current

$$c = k\left[gh\left(\frac{\Delta\bar{\theta}}{\theta_0}\right)\right]^{1/2}, \qquad (1)$$

where c is the propagation speed of the density current, k is an empirically determined Froude number, g is gravity, h is the depth of the current (generally taken as the height of the flow far behind the current head), $\Delta\bar{\theta}$ is the potential temperature contrast across the interface or over the current depth h, and θ_0 is the mean potential temperature.

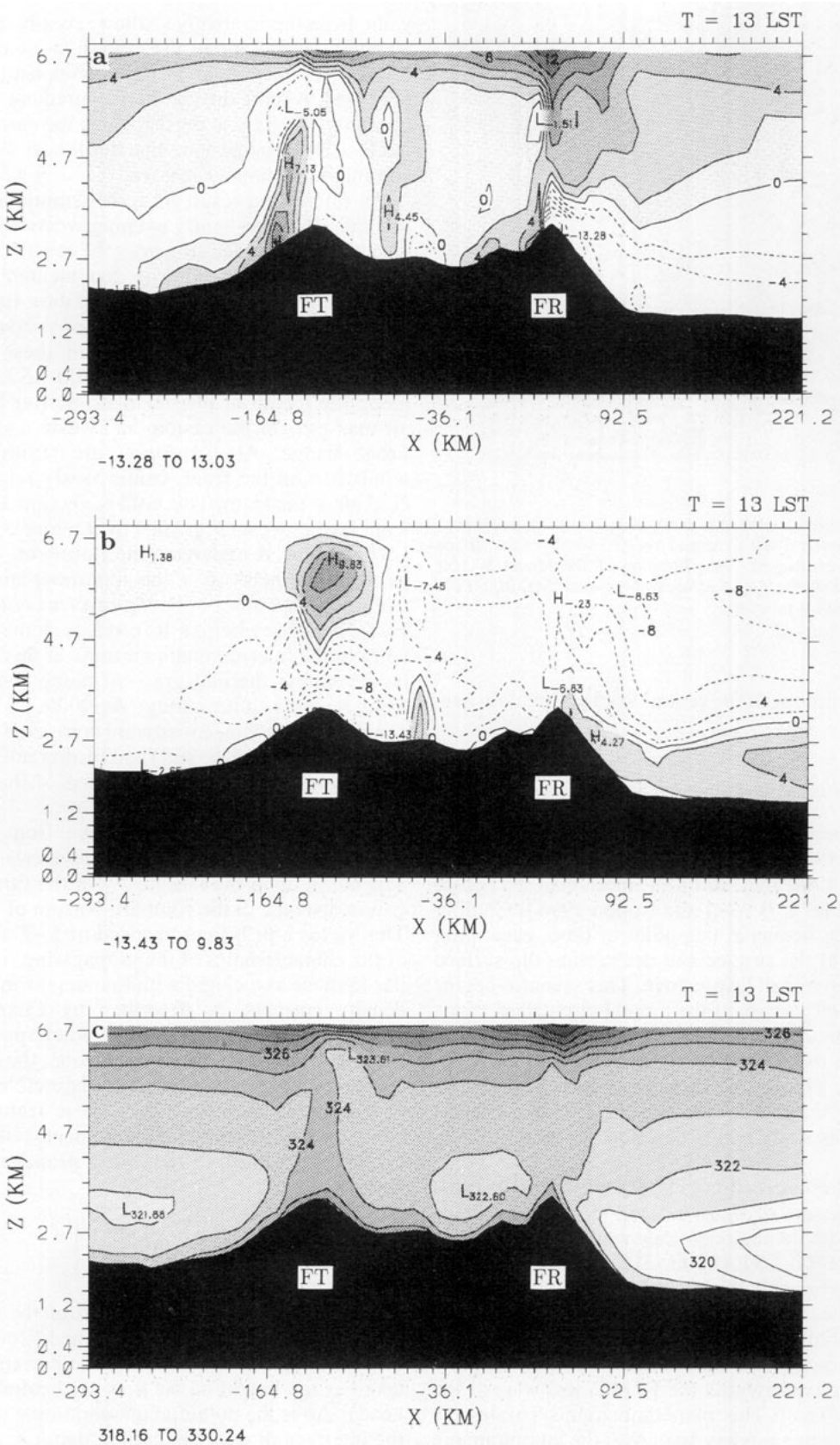

FIG. 8. Vertical cross sections of (a) u-component wind (contour interval 2 m s^{-1}), (b) v-component wind (contour interval 2 m s^{-1}), and (c) potential temperature θ (contour interval 1.0°C) on grid 3 at 40.0°N for 1300 LST 26 August 1985. Location of the Flat Tops (FT) and Front Range (FR) indicated for reference.

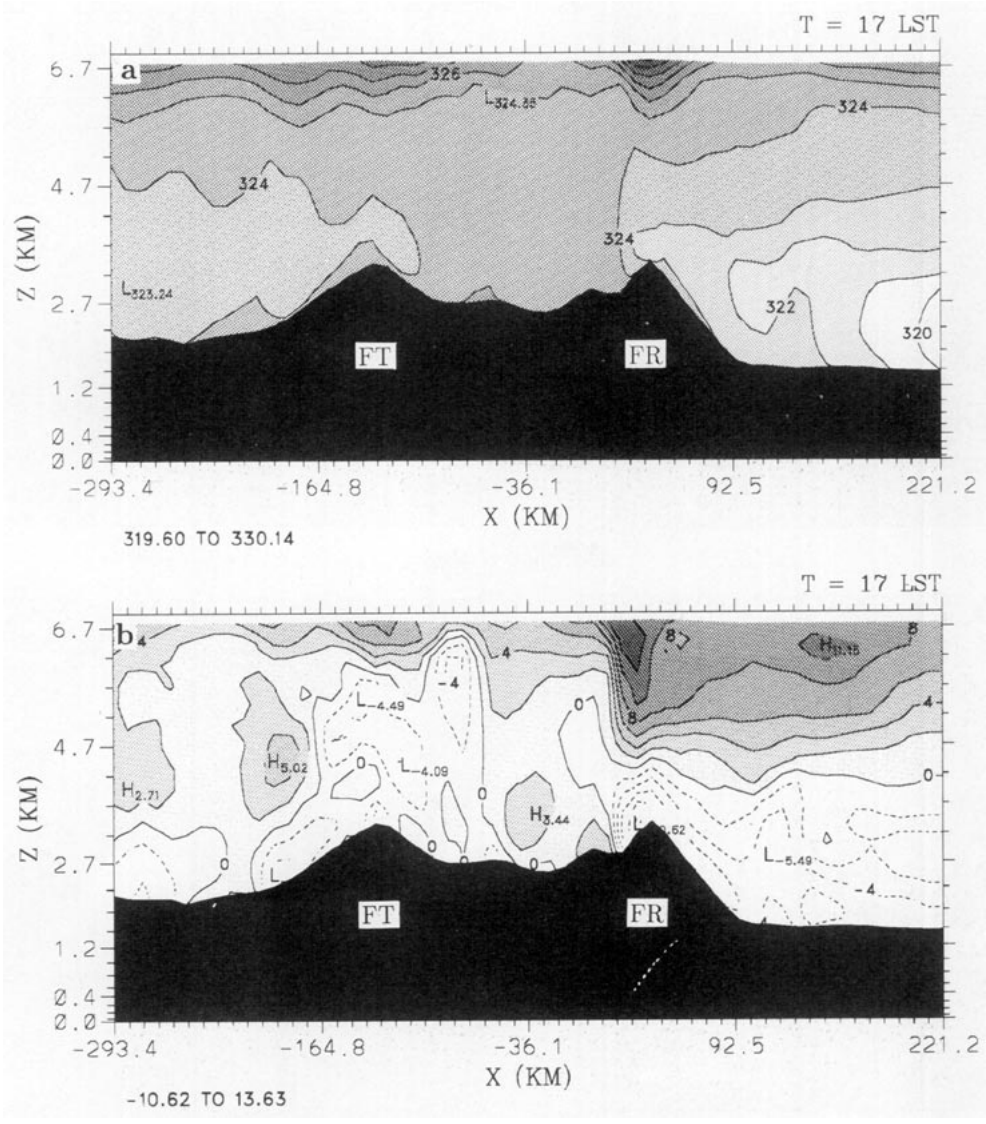

FIG. 9. Vertical cross sections of (a) potential temperature θ (contour interval 1.0°C) and (b) u-component wind (contour interval 2 m s^{-1}) on grid 3 at 40.0°N for 1700 LST 26 August 1985. Location of the Flat Tops (FT) and Front Range (FR) indicated for reference.

For the calculation of the density current phase speed in the model simulation, we have chosen to look at various west–east cross sections at 1900 LST to determine an appropriate average depth and temperature difference across the frontal interface. While quite variable over the complex model topography, appropriate values for the parameters are $\Delta\bar{\theta} \approx 2.0$ K, $\theta_0 = 323$ K, $h = 700$–1000 m, $k = 1$, and $g = 9.81$ m s^{-2}, which yields a current speed of 6.5–7.8 m s^{-1}, within the range of the simulated propagation speed, given the approximate nature of the calculation. Although this calculation does not include any effects of the sloping terrain over which the front propagates, Britter and Linden (1980) have shown that the primary influence of sloping terrain on density currents is not to increase the current propagation speed but rather to increase the depth of the current through entrainment. Thus, it appears that the potentially cooler air from east of the barrier crest propagates westward in the late afternoon as a density current. Henceforth, we shall refer to this westward-propagating density current as the WPDC for brevity.

c. *Simulated nocturnal circulations*

The leading edge of the WPDC propagates to the western edge of the Colorado mountains by 2200 LST. In the wake of the WPDC, southerly flow develops over the intermountain region, while over the eastern and western slopes divergent near-surface flow away from

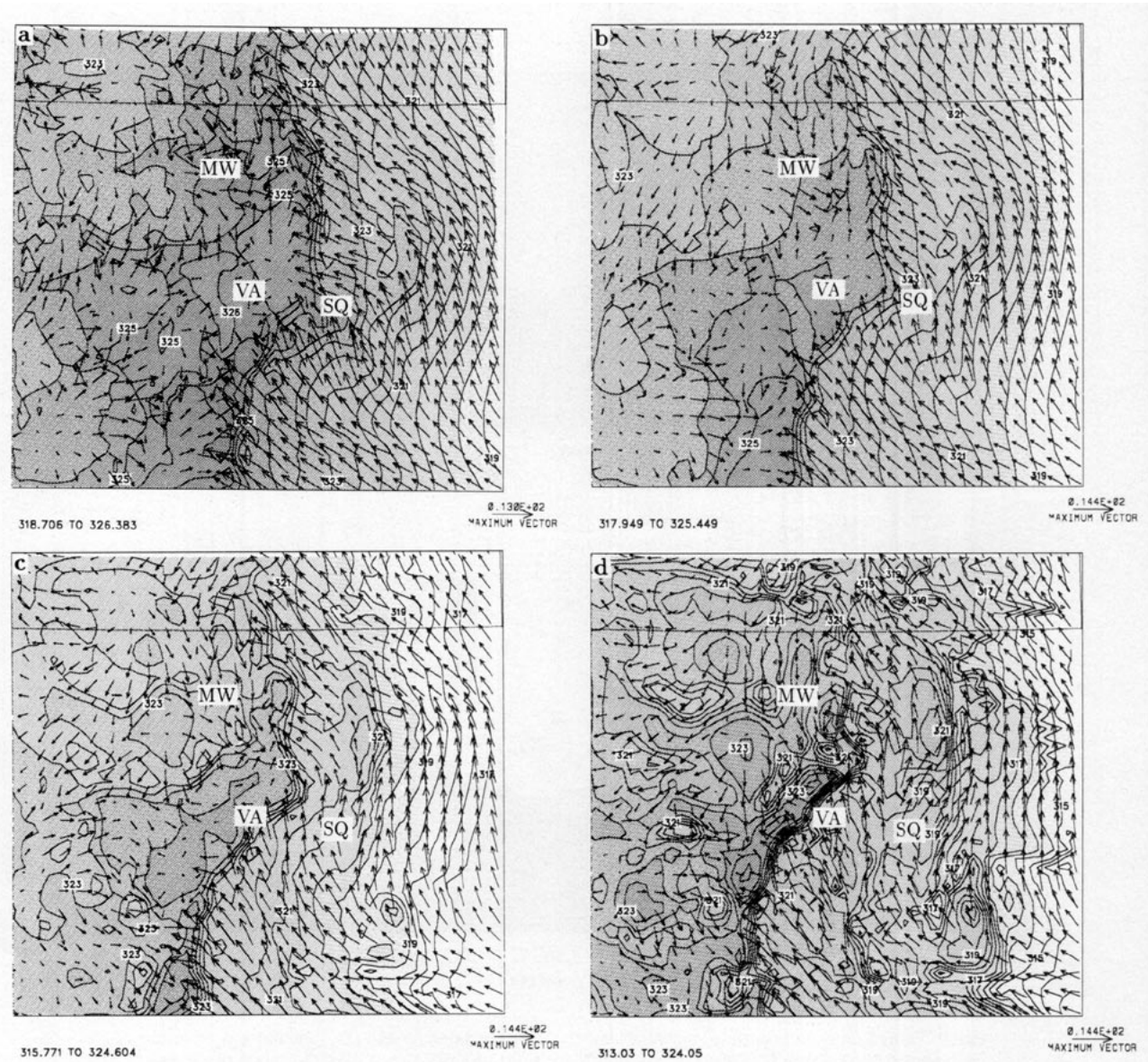

FIG. 10. Wind vectors at every other grid point and potential temperatures (contour interval 1.0°C) on grid 3 at 50 m above the surface for (a) 1700 LST, (b) 1800 LST, (c) 1900 LST, and (d) 2000 LST 26 August 1985. Locations of the Mount Werner (MW), Vail Mountain (VA), and Squaw Mountain (SQ) ROMPEX stations indicated for reference.

the highest terrain becomes well established due to the influence of radiative cooling over the respective slopes. These events signal the onset of the nocturnal outflow wind regime across the mountain barrier on this case day. The simulated wind field at 0100 LST (Fig. 11a) shows southwesterly flow along the entire eastern slope of the Front Range. Over the intermountain region, steady southerly flow persists, with some rotation toward the southwest indicated. This gradual veering of the flow continues through the remainder of the simulation (Fig. 11b). The steadiness of the late night south-southwest flow over the intermountain region suggests that a balance has been achieved between the westward-directed pressure gradient and eastward-oriented Coriolis acceleration. The influence of surface friction, generally an important component of the force balance, is diminished due to the highly stratified near-surface conditions that exist over the intermountain region during this nocturnal period.

At the end of the simulation (0500 LST 27 August 1985), upper-level winds on grid 1 show that the general upper-level wind pattern over the central Rocky Mountains is from a south-southwest direction, due to the movement of the upper-level ridge from west to east of the mountain barrier during this 24-h period (Fig. 12a). In general, the large-scale features within

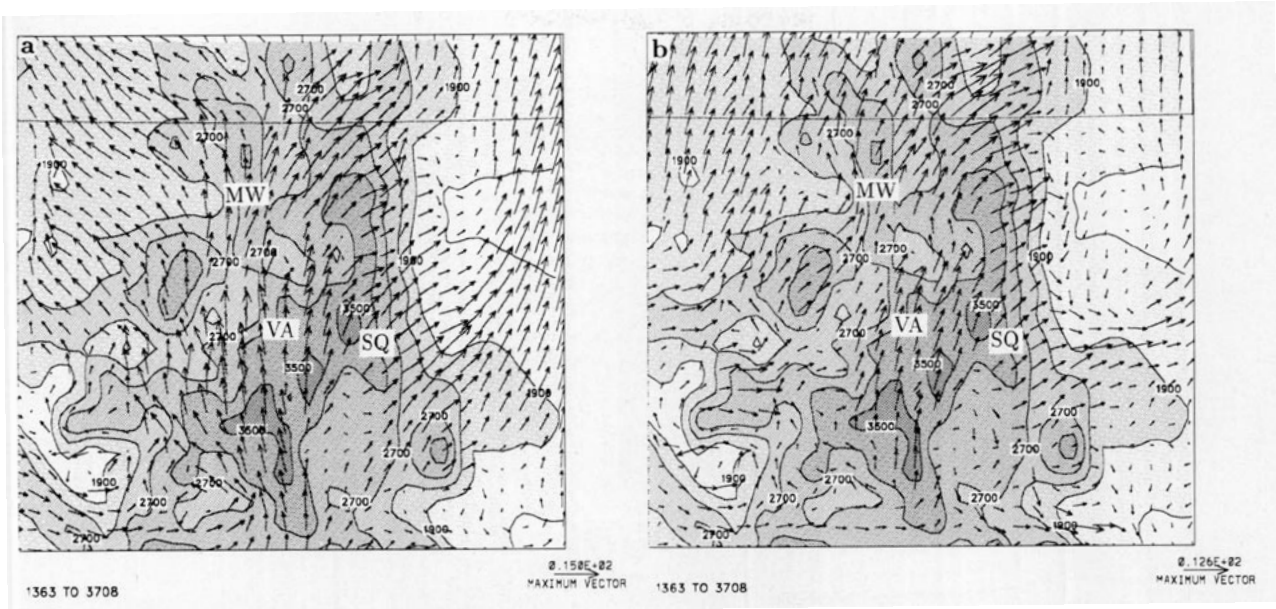

FIG. 11. Wind vectors at every other grid point on grid 3 at 278 m above the surface for (a) 0100 LST and (b) 0500 LST 27 August 1985. Locations of the Mount Werner (MW), Vail Mountain (VA), and Squaw Mountain (SQ) ROMPEX stations indicated for reference.

the simulated upper-level flow are in good agreement with those observed, especially over Colorado, as indicated by the southwesterly winds at the two rawinsonde stations (see Fig. 3b). Near the surface (Fig. 12b), the flow over Colorado is similar to that of the previous day at the same time (see Fig. 5b), except that the winds here are weaker and from a more southwesterly direction. These results suggest that the model has done an adequate job of simulating the observed regional- to large-scale conditions within the region of interest over this 36-h period.

d. Observation and model simulation comparisons

In Fig. 13, wind direction and wind speed time series from four ROMPEX ground stations located in the various geographical regions of the Colorado mountain barrier (e.g., Front Range east slope, Front Range crest, intermountain region, western slope of the barrier; see Fig. 1) are compared with time series from the lowest model level (~50 m) for the grid point on grid 3 nearest to each station. These time series span the 24-h period beginning at 0500 LST 26 August and ending at 0500 LST 27 August.

The eastern slope of the Front Range is represented in Fig. 13a by Squaw Mountain (SQ in Fig. 1, at 3505 m MSL). Here, the simulation–observation comparison shows that the overall eastern slope diurnal wind cycle is captured in the model. Differences exist, however, in the timing of the wind shifts between upslope and downslope flow, and in the wind speeds that are systematically too high in the simulation. Despite these problems, the model simulates well the morning westerly flow, the shift to an afternoon easterly component upslope flow, and the evening shift back to downslope flow, and ends up with southwesterly flow in agreement with the observed winds. While the wind speeds are excessive, the model does show some of the same trends in wind speed during each component of the wind direction cycle and the transitions between them.

It is important to note that the simulated winds shown are an average of the speed over the first 100 m above the surface, and the observed winds are from 3 m. Unfortunately, no measured vertical profiles of the slope wind regime are available. Fitting the simulated winds shown in Fig. 13a at approximately 50 m, the lowest model level, to a log wind profile to get the speeds at 3 m can account for a 50% speed decrease. Also, the simulated speeds are instantaneous values (which might account for the high daytime variability), while the observed speeds are hour averages. In addition, the model surface is a highly smoothed representation of the actual terrain, which has many subgrid topography, roughness, soil, and vegetation variations that are not included in this simulation, with a maximum 7-km horizontal resolution. In particular, the model's surface is relatively smooth, consisting of bare dirt with a constant roughness $z_0 = 0.04$ m specified over the entire model domain. While an obvious simplification, these parameters were chosen due to the lack of sufficient land-use characterization data available.

Simulation and observational comparisons at the crest of the Front Range are provided in Fig. 13b for the Rocky Mountain National Park location (RM in Fig. 1, at 3660 m MSL). Again, the simulation captures very well the diurnal wind direction cycle at this location, with the exception of the westerly to easterly

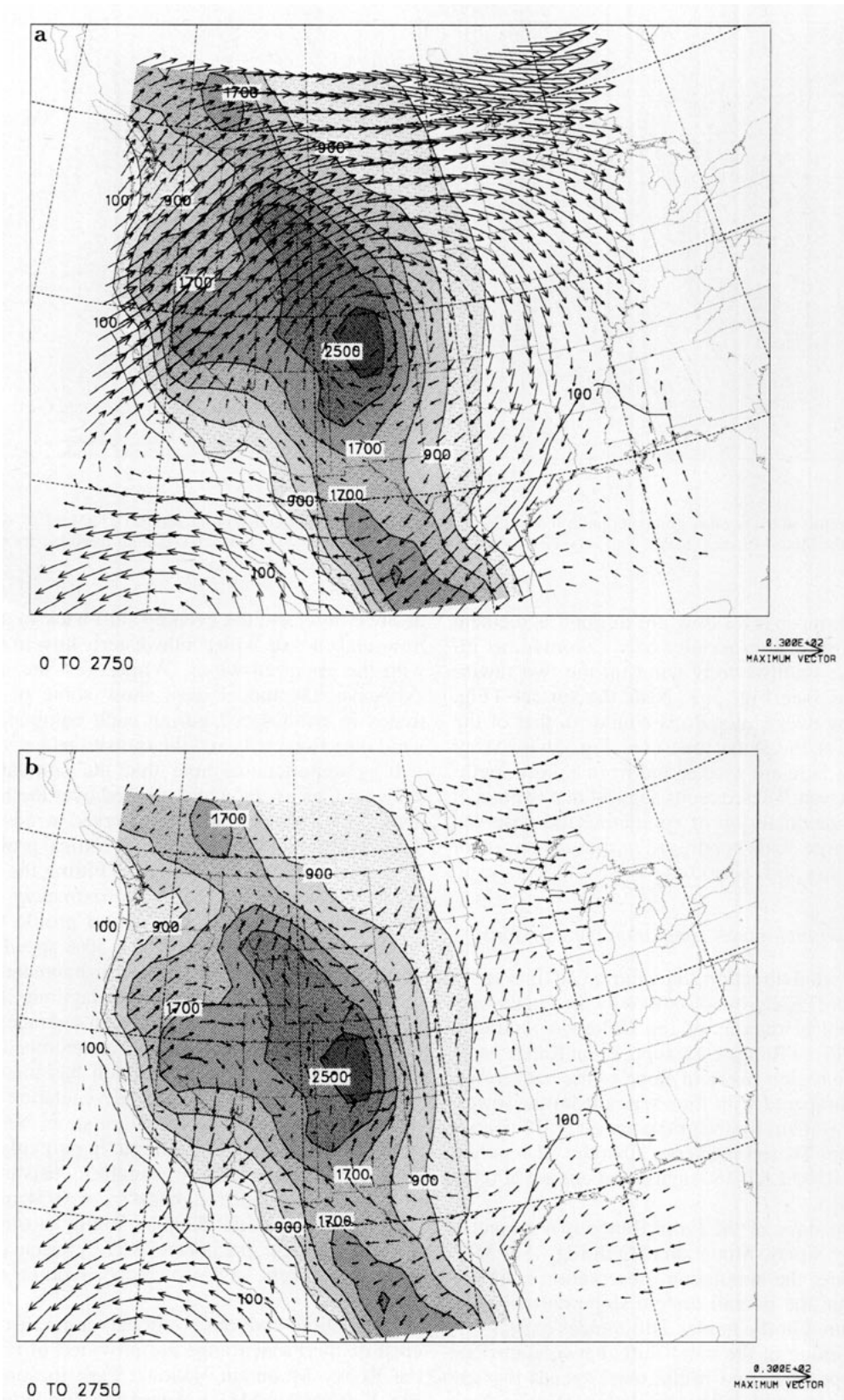

FIG. 12. Wind vectors at every grid point and topography (contours every 400 m) on grid 1 at (a) 5.65 km AGL and (b) 0.05 km AGL for 0500 LST (1200 UTC) 27 August 1985.

component transition, which is 2 h early in the simulation, although consistent with the earlier transition to upslope flow noted in Fig. 13a. Wind speeds are very comparable between the model and the observations until the onset of the easterly component flow, which is significantly higher in the simulation, although the trend for a delayed maximum in speed after the onset of the easterly winds and the decreasing speeds thereafter are similar to those observed. After the late afternoon and early evening period of easterly component flow, the tendency for the wind direction to remain from a south-southwest direction throughout the night is also captured in the simulation.

Within the intermountain region, we compare the simulation with the ground station at Vail Mountain (VA in Fig. 1, at 3350 m MSL) and again find a strong correlation between the simulated and observed diurnal wind direction (Fig. 13c). In particular, both cycles show a shift in midmorning to west-northwest flow that persists until early evening, at which time the wind shifts to easterly component flow and increases in speed. The timing of this event is again 2 h earlier in the simulation than was observed. The wind shift marks a transition to a steady nocturnal flow regime from the south-southeast in the model and from the southeast in the mountaintop observations. Wind speeds, while significantly higher in the simulation, show a high degree of correlation with those observed: both trend toward a daytime maxima, a transitional minima, and a wind surge with the onset of the nocturnal regime.

The final comparison (Fig. 13d) takes place at the western edge of the Colorado mountain barrier at Mount Werner (MW in Fig. 1, at 3207 m MSL). While the observed wind direction is more variable than at the other stations, the overall comparison is similar. Both winds are from a westerly direction until 2000 LST, when the simulated winds undergo a shift to northeasterly flow. After 3 h, the simulated northeasterly winds are followed by a wind shift to south-southeast flow that persists throughout the remainder of the comparison, similar to Vail Mountain (Fig. 13c). The observed winds, on the other hand, remain from a westerly component direction until 2200 LST when a shift to southerly flow briefly occurs, after which westerly component flow returns for 2 h before the observed winds shift to south-southeast flow for the remainder of the evening. The simulated wind speeds are consistently higher than the very weak winds that were observed. The highest speeds in both cases occur during the onset of the southerly component flow regime.

Despite an apparent overprediction of wind speed within this case day simulation, the comparisons in Fig. 13 demonstrate that the simulated flow behavior is consistent with the ROMPEX observations. Of particular interest to this study are the development of the FRMC along the eastern slope of the Front Range, its transition to a WPDC, and the propagation times of the WPDC between the various sites. While the model overpredicts the strength of the low-level branch of the FRMC and advects the easterly flow through each station 2 h earlier than observed, the propagation speed of the WPDC is well simulated, since the 2-h difference is systematic between each station. In addition, the model captures the diurnal wind shifts at each station, as well as the steady late night wind direction in every case. Considering that the wind behavior shown here is a 12–36-h prediction at actual ground station locations in highly complex terrain, we find the comparisons to be very convincing and feel that the simulation presents a realistic overall depiction of the actual regional-scale wind circulations that occurred on the case day.

6. Discussion and conceptual model

Regional-scale wind patterns across the Colorado mountains have been investigated with a three-dimensional numerical simulation, initialized with observed data. The study compared the simulated circulation systems with actual conditions at mountaintop stations across the Colorado mountain barrier for a particular case day. This case day simulation has shown that the general characteristics of the diurnal evolution of regional-scale circulations over the central Rocky Mountains are included within the simulation. In addition, however, the model is able to simulate many aspects of the circulation evolution that go beyond those that could be deduced from the ground-based observed data. In particular, the model simulates the transformation in late afternoon of the FRMC into a WPDC. This WPDC was not a feature of our original inflow–outflow conceptual model discussed in section 1 and in Bossert et al. (1989). From the present study, four primary stages of a regional-scale circulation system have been identified. In the ensuing discussion, we focus primarily on describing the circulation as it appears at 40°N.

a. Daytime mountain boundary-layer development phase

The most important thermally forced flow feature within the simulation was the mountain–plains circulation along the eastern slope of the Front Range (i.e., the FRMC, Fig. 14). This circulation system consists of a pressure–density solenoid (Holton 1979) with a low-level upslope branch, vertical branch, and outflow or return branch at 5–6 km AGL. Similar, though generally weaker, thermally direct circulation systems exist over the many smaller mountain ranges comprising the western slope of the Colorado Rocky Mountains, giving a mean westerly low-level inflow component toward the Continental Divide.

The vertical branch of the FRMC delineates the boundary between two differentially heated air masses. A baroclinic zone results between the heated air within the mixed layer over the intermountain region west of

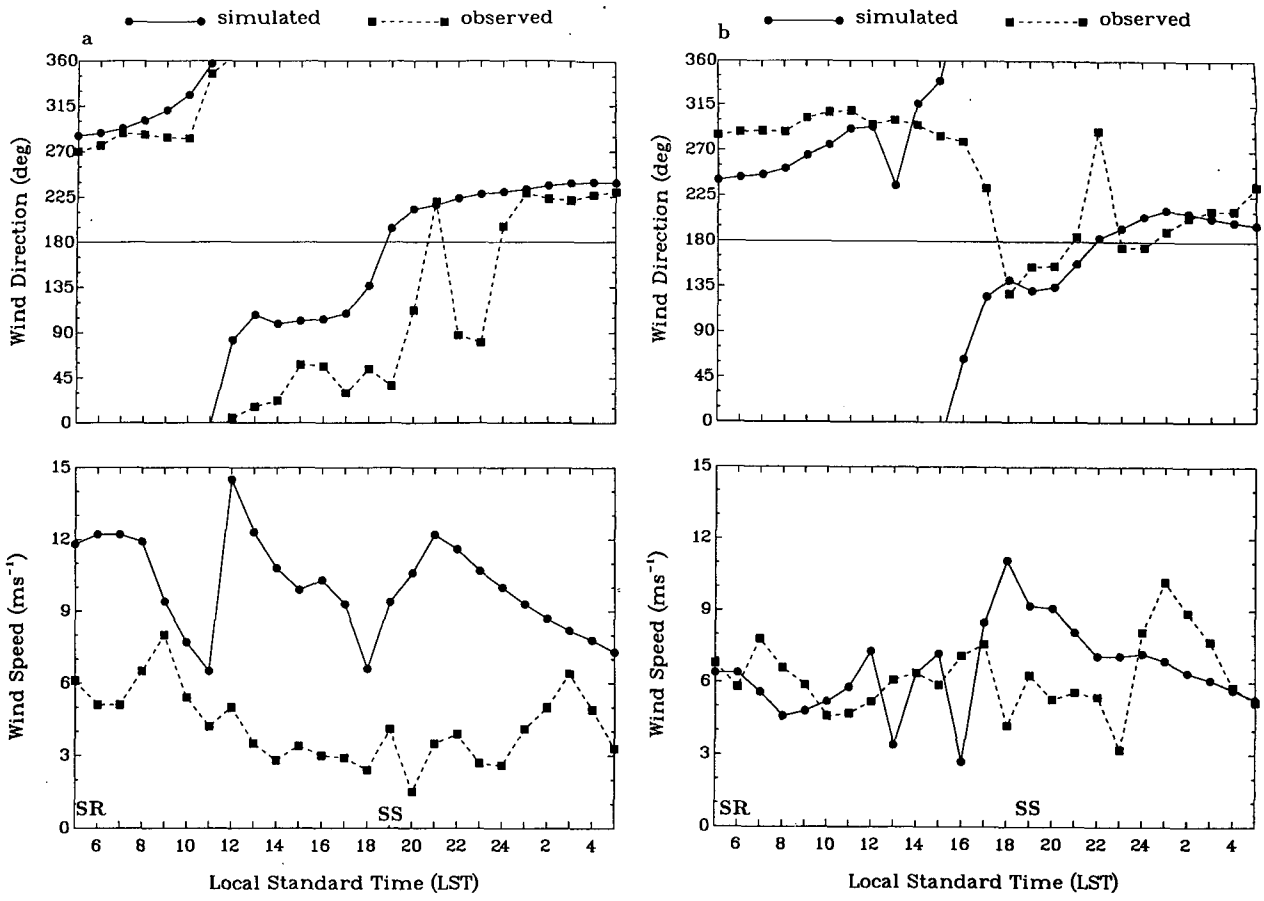

FIG. 13. Simulated and observed wind direction for (a) SQ (eastern slope), (b) RM (barrier crest), (c) VA (intermountain region), and (d) MW (western edge of the mountain massif) locations from 0500 LST 26 August to 0500 LST 27 August 1985. (See Fig. 1 for actual station locations.) The labels SR and SS show the approximate time of sunrise and sunset, respectively.

the Front Range and the unheated air at a similar altitude above the mixed layer east of the Front Range barrier. This thermal front is intensified throughout the late morning and early afternoon by continued surface heating and convergence of upslope flows at the barrier crest.

b. Late-afternoon transition phase

By late afternoon, the baroclinicity across the FRMC peaks from the sustained differential heating. Weakening of the convergent flow in the low-level branch of the circulation system occurs concurrently from diminished surface forcing. At this time, the regional-scale temperature contrast across the Front Range barrier overwhelms the heating-induced convergence over each slope, forcing the potentially cooler air within the FRMC from its initial position near the Front Range crest westward over the barrier and down the western slope (Fig. 15). By this time, low-level winds within the FRMC are from the southeast due to prolonged influence of the Coriolis force upon the circulation system (see Fig. 10a). Coriolis effects throughout the diurnal cycle adjust the evolving circulation system gradually toward geostrophic balance. The manifestation of this adjustment is a low-level cyclonic circulation across the baroclinic zone and an anticyclonic circulation near the top of the boundary layer between 2 and 3 km AGL, both of which can be seen in their incipient phases in Figs. 8a,b and which will progressively encompass the entire west–east extent of the Colorado mountain barrier.

As the FRMC propagates over the barrier crest it begins to collapse from its negative buoyancy and the demise of surface heating, gradually transforming into a more shallow, intrusive current within the deep boundary layer over the intermountain region. Once the transforming FRMC begins to propagate into the intermountain region, it takes on the physical characteristics of a density current as defined by Benjamin (1968), Simpson (1969), Charba (1974), Goff (1976), and many others. The evolution of the FRMC into a much shallower westward-propagating density current (WPDC) circulation is a widespread event and encom-

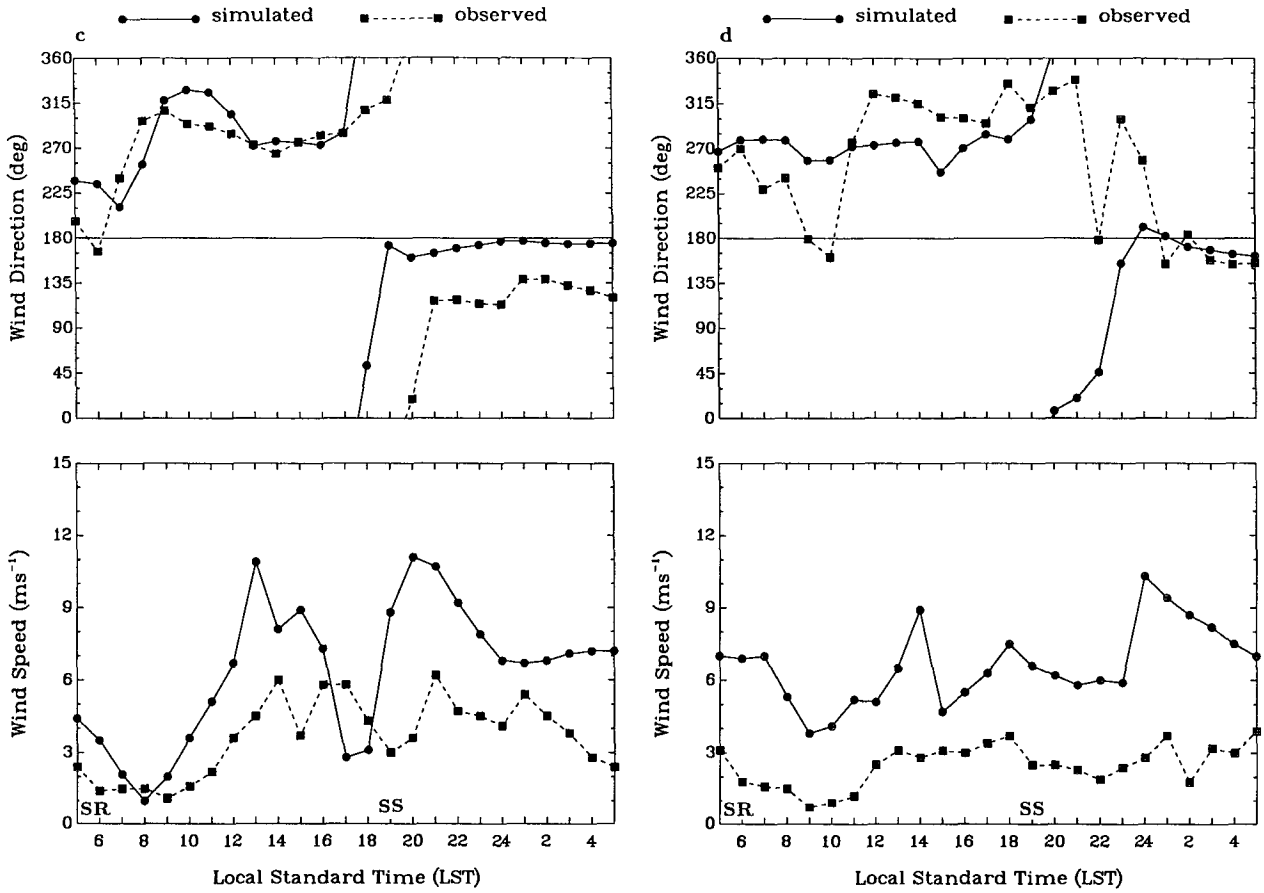

FIG. 13. (*Continued*)

passes the entire north–south extent of the eastern slope of Colorado within the model simulation and probably occurs in other preferential locations along the Rocky Mountain–Great Plains interface. Conditions for the development of this FRMC–WPDC system are described in more detail in Bossert and Cotton (1994).

West of the Front Range crest, the WPDC causes an abrupt shift in the winds from west-northwest flow, characteristic of the daytime wind regime, to strong southeasterly flow. Thus, the abrupt wind shift appears as a progressive phenomenon in agreement with the ROMPEX observations over the western slope. Concurrent with the evolution of the WPDC in late afternoon, the upslope flow regime along the eastern slope decays and, with the onset of radiative surface cooling in the early evening, begins to veer toward a downslope direction.

This unusual transitional flow behavior over the Colorado mountains appears to have an analog in northern Australia. There, the propagation of the east coast sea-breeze front over the crest of the Cape York Peninsula and its subsequent transformation into a density current has been described by Clarke (1972, 1983a,b, 1984), Crook and Miller (1985), and others. This density current is the precursor to the well-known "morning glory" phenomenon (Clarke 1965).

c. *Evening density-current propagation phase*

The nocturnal phase of the regional-scale circulation system over the Colorado mountain barrier generally begins once the WPDC has propagated the length of the intermountain region and subsequently shifted the flow along the western slope from an inflow (westerly component) to outflow (easterly component) direction (Fig. 16). Topographic channeling and continuing Coriolis influence act to rotate the once southeasterly flow toward a more southerly direction. After it reaches the edge of the high terrain, the head of the current separates from the core of the flow and decays away over the lower terrain of western Colorado. Although not shown, the demise of the current over western Colorado appears similar to the decay of a far inland penetrating sea-breeze front into an isolated vortex, observed near dawn in northern Australia, as described and simulated by Physick and Smith (1985).

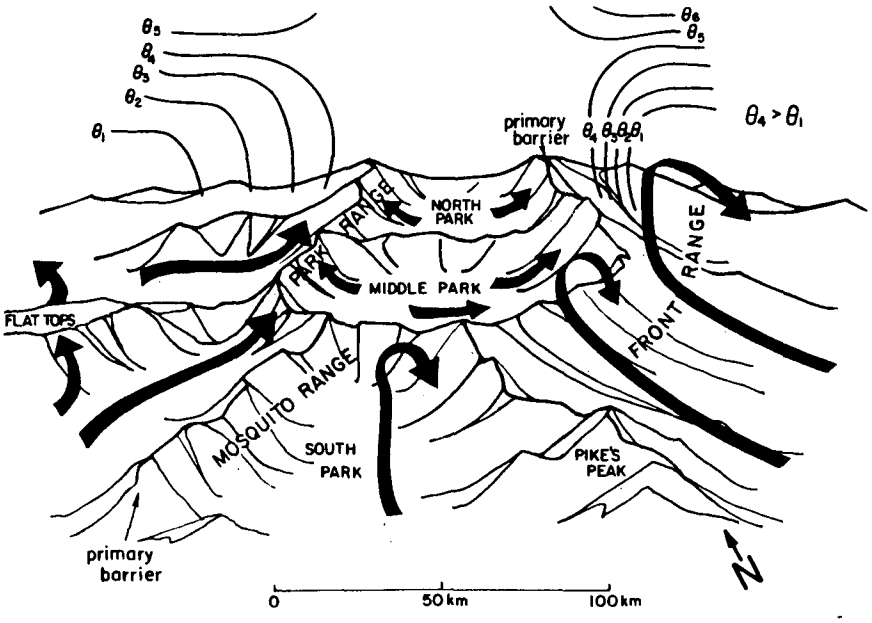

FIG. 14. Conceptual model of the regional-scale daytime inflow circulation system over the north-central Colorado Rocky Mountains.

d. Late-night adjustment phase

Late at night, the nocturnal flow over north-central Colorado consists of shallow downslope flows along the major slopes of the complex topography and a regional-scale adjusted southerly jet through the intermountain region. While the downslope flows evolve in response to thermal imbalances induced by radiative cooling on a spatial scale the order of individual slopes, the widespread southerly flow is the geostrophically balanced response to the mesoscale thermal gradient that continues to persist in the lower troposphere between the colder eastern (higher pressure) and warmer western (lower pressure) sides of the mountain barrier. This scenario of prevailing southerlies over the center of the intermountain region in a quasi-balanced state

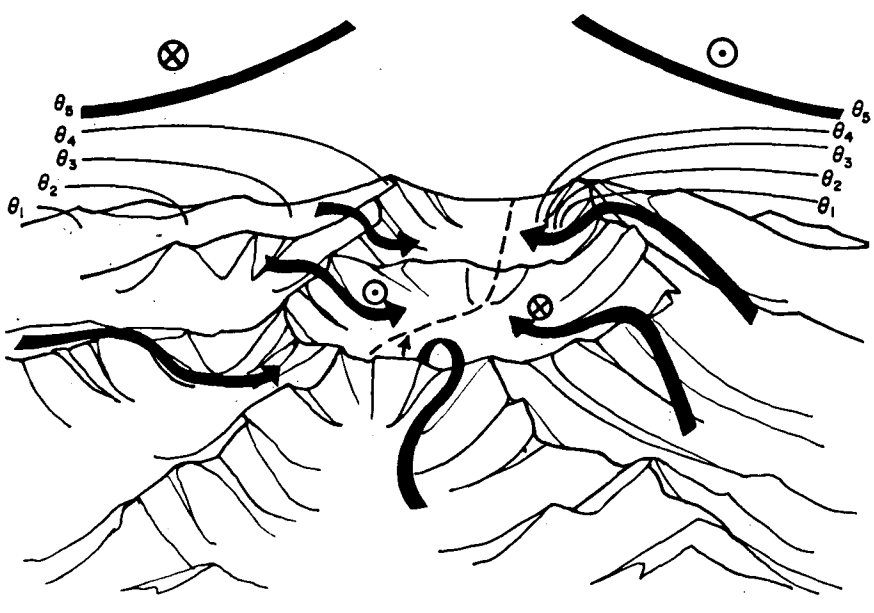

FIG. 15. Transition phase conceptual model of the regional-scale circulation system over the north-central Colorado Rocky Mountains.

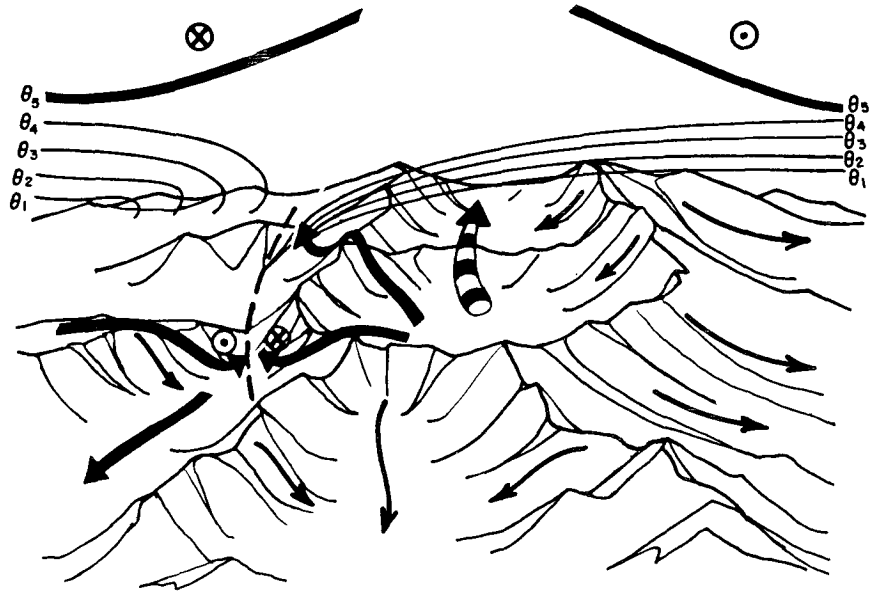

FIG. 16. Conceptual model of the regional-scale nocturnal outflow circulation system over the north-central Colorado Rocky Mountains.

persists until the onset of heating the following morning.

7. Conclusions

A wind regime with distinct diurnally reversing flow characteristics has been observed to occur with regularity over the Colorado mountain barrier. Coherent flow structure at mountaintop stations indicate that this flow regime is of meso-β- to meso-α-scale proportions or regional scale, thus occupying a discrete spatial scale within the hierarchical order of thermally induced circulation systems over complex terrain. The most unusual observed feature of this wind regime in Colorado was the steady, high-speed nocturnal easterly component winds observed at mountaintop level (70 kPa) along the western slope of the mountain barrier. These easterly winds were generally from a direction counter to the ambient westerly component flow and, though widespread over the mountains, were unresolved within the existing rawinsonde network.

The case day simulation with the RAMS mesoscale model captured the diurnal evolution of the low-level mountain boundary-layer circulation development, as shown in comparisons with the ROMPEX observations. The simulation revealed the complex transformation in late afternoon of the thermally driven, regional-scale circulation along the eastern slope of the mountain barrier from a deep, contiguous, mountain–plains solenoid (the FRMC) to a more shallow, westward-propagating density-current circulation (the WPDC). The strong low-level winds associated with the WPDC provided the forcing mechanism responsible for the abrupt flow reversal to strong nocturnal southeasterly winds observed at mountaintop over the western slope. The WPDC dissipated near midnight along the western edge of the Colorado mountain massif, leaving in its wake a steady low-level (1–2 km AGL) southerly jet that resulted from the prolonged influence of the Coriolis force on the FRMC and WPDC circulations, which are the thermally direct response to the induced cross-barrier temperature gradient. This geostrophically balanced flow over the high mountain terrain constitutes the final stage of the diurnal regional-scale circulation across the Colorado mountain barrier. Shallow downslope flows occur over the resolvable slopes beneath the balanced southerly flow.

Further studies will be necessary to examine the influence of external forcing mechanisms on the development of the flow regimes described in this research, in an effort to more clearly define the parameter space in which these circulation systems can exist. Some of these mechanisms will be addressed in a companion paper (Bossert and Cotton 1994). The feedback between the flow regime described herein and deep moist convection over the Colorado mountains is another topic that will be examined in future research. The implications of this regional-scale flow phenomenon on the dispersion of pollutants from along the Front Range is also a topic worthy of additional study.

Acknowledgments. Most of this research was performed while the first author was a graduate student in the Department of Atmospheric Science at Colorado State University, supported by a fellowship from the

Army Research Office (ARO) Center for Geosciences, Contract DAAL03-86-K-0175. The work was finalized at the Los Alamos National Laboratory, which is managed by the University of California under the auspices of the Department of Energy. The numerical simulation was performed on the CRAY-XMP at the National Center for Atmospheric Research (NCAR). NCAR is sponsored by the National Science Foundation. The observational portion of this research was sponsored by the National Aeronautics and Space Administration under Grant NAGW601, by the National Science Foundation under Grant ATM-86-10796, by the Air Force Office of Scientific Research, Air Force Systems Command Grant F49620-85-C-0077DEF, and by the U.S. Department of Energy's Atmospheric Studies in Complex Terrain (ASCOT) Program under the University of California, Los Alamos National Laboratory Subcontract 9-X38-5759V-1. Special thanks are owed to Profs. Thomas B. McKee and Elmar R. Reiter for facilitating the numerical and observational portions of this work, respectively, and for the benefit of their insight. In addition, the numerical modeling was aided by Drs. Craig J. Tremback and Robert L. Walko, and by Peter Q. Olsson. The entire study benefited tremendously from discussions, suggestions, and criticisms from Dr. Jerome M. Schmidt, John D. Sheaffer, Dr. C.-Y. Jim Kao, Dr. Michael Moran, and Ray McAnelly.

REFERENCES

Atkinson, B. W., 1981: *Meso-scale Atmospheric Circulations.* Academic Press, 495 pp.

Bader, D. C., T. B. McKee, and G. J. Tripoli, 1987: Mesoscale boundary layer evolution over complex terrain. Part I: Numerical simulation of the diurnal cycle. *J. Atmos. Sci.,* **44,** 2823–2838.

Banta, R. M., and W. R. Cotton, 1981: An analysis of the structure of local wind systems in a broad mountain basin. *J. Appl. Meteor.,* **20,** 1255–1266.

Barnes, S. L., 1973: Mesoscale objective map analysis using weighted time series observations. NOAA Tech. Memo. ERL NSSL-62, 66 pp. [NTIS COM-73-10781.]

Barry, R. G., 1992: *Mountain Weather and Climate.* 2d ed. Routledge, 402 pp.

Benjamin, T. B., 1968: Gravity currents and related phenomena. *J. Fluid Mech.,* **31,** 209–248.

Bossert, J. E., 1990: Regional-scale flows in complex terrain: An observational and numerical investigation. Ph.D. dissertation, Colorado State University, 254 pp. [Available from University Microfilms, Ann Arbor, MI 48106.]

——, and E. R. Reiter, 1987: Observed characteristics of a mountain-plain circulation in Colorado. *Proc. AMS Fourth Conf. on Mountain Meteorology,* Seattle, WA, Amer. Meteor. Soc., 20–21.

——, and W. R. Cotton, 1994: Regional-scale flows in mountainous terrain. Part II: Simplified numerical experiments. *Mon. Wea. Rev.,* **122,** 1472–1489.

——, J. D. Sheaffer and E. R. Reiter, 1989: Aspects of regional-scale flows in mountainous terrain. *J. Appl. Meteor.,* **28,** 590–601.

Britter, R. E., and P. F. Linden, 1980: The motion of the front of a gravity current travelling down an incline. *J. Fluid Mech.,* **99,** 531–543.

Charba, J., 1974: Application of gravity current model to analysis of squall line gust front. *Mon. Wea. Rev.,* **102,** 140–156.

Chen, C., and W. R. Cotton, 1983: A one-dimensional simulation of the stratocumulus-capped mixed layer. *Bound.-Layer Meteor.,* **25,** 289–321.

Clark, T. L., and R. D. Farley, 1984: Severe downslope windstorm calculations in two and three spatial dimensions using anelastic interactive grid nesting: A possible mechanism for gustiness. *J. Atmos. Sci.,* **41,** 329–350.

Clarke, R. H., 1965: Horizontal mesoscale vortices in the atmosphere. *Aust. Meteor. Mag.,* **50,** 1–25.

——, 1972: The morning glory: An atmospheric hydraulic jump. *J. Appl. Meteor.,* **11,** 304–311.

——, 1983a: Fair weather nocturnal inland wind surges and atmospheric bores. Part I: Nocturnal wind surges. *Aust. Meteor. Mag.,* **31,** 133–145.

——, 1983b: Fair weather nocturnal inland wind surges and atmospheric bores. Part II: Internal atmospheric bores in northern Australia. *Aust. Meteor. Mag.,* **31,** 147–160.

——, 1984: Colliding sea-breezes and the creation of internal atmospheric bore waves: Two-dimensional numerical studies. *Aust. Meteor. Mag.,* **32,** 207–226.

Cotton, W. R., and R. A. Anthes, 1989: *Storm and Cloud Dynamics.* Academic Press, 883 pp.

Crook, N. A., and M. J. Miller, 1985: A numerical and analytical study of atmospheric undular boles. *Quart. J. Roy. Meteor. Soc.,* **111,** 225–242.

Davies, H. C., and R. E. Turner, 1977: Updating prediction models by dynamic relaxation: An examination of the technique. *Quart. J. Roy. Meteor. Soc.,* **103,** 225–245.

Defant, F., 1951: Local winds. *Compendium of Meteorology,* Amer. Meteor. Soc., 655–672.

Doran, J. C., and S. Zhong, 1994: Regional drainage winds in the Pacific Northwest. *Mon. Wea. Rev.,* **122,** 1158–1167.

Goff, R. C., 1976: Vertical structure of thunderstorm outflows. *Mon. Wea. Rev.,* **104,** 1429–1440.

Holton, J. R., 1979: *An Introduction to Dynamical Meteorology.* 2d ed. Academic Press, 391 pp.

Jeffreys, H., 1922: On the dynamics of the wind. *Quart. J. Roy. Meteor. Soc.,* **48,** 29–47.

Klemp, J. B., and R. B. Wilhelmson, 1978a: The simulation of three-dimensional convective storm dynamics. *J. Atmos. Sci.,* **35,** 1070–1096.

——, and ——, 1978b: Simulations of right- and left-moving storms produced through storm splitting. *J. Atmos. Sci.,* **35,** 1097–1110.

Louis, J. F., 1979: A parametric model of vertical eddy fluxes in the atmosphere. *Bound.-Layer Meteor.,* **17,** 187–202.

Mass, C., 1982: The topographically forced circulations of western Washington State and their influence on precipitation. *Mon. Wea. Rev.,* **110,** 170–183.

Physick, W. L., and R. K. Smith, 1985: Observations and dynamics of sea-breezes in northern Australia. *Aust. Meteor. Mag.,* **33,** 51–63.

Pielke, R. A., W. R. Cotton, R. L. Walko, C. J. Tremback, W. A. Lyons, L. D. Grasso, M. E. Nicholls, M. D. Moran, D. A. Wesley, T. J. Lee, and J. H. Copeland, 1992: A comprehensive meteorological modeling system—RAMS. *Meteor. Atmos. Phys.,* **49,** 69–91.

Reiter, E. R., J. D. Sheaffer, J. E. Bossert, R. C. Fleming, W. E. Clements, J. T. Lee, S. Barr, J. A. Archuleta, and D. E. Hoard, 1987: ROMPEX—The Rocky Mountain Peaks Experiment of 1985: Preliminary assessment. *Bull. Amer. Meteor. Soc.,* **68,** 321–328.

Sheaffer, J. D., and E. R. Reiter, 1987: Measurements of surface energy budgets in the Rocky Mountains of Colorado. *J. Geophys. Res.,* **92,** 4145–4162.

Simpson, J. E., 1969: A comparison between laboratory and atmospheric density currents. *Quart. J. Roy. Meteor. Soc.,* **95,** 754–765.

Staley, D. O., 1957: The low-level sea breeze of northwest Washington. *J. Meteor.,* **14,** 458–470.

Tang, M., and E. R. Reiter, 1984: Plateau monsoons of the Northern Hemisphere: A comparison between North America and Tibet. *Mon. Wea. Rev.,* **112,** 617–637.

Toth, J. J., and R. H. Johnson, 1985: Summer surface flow characteristics over northeast Colorado. *Mon. Wea. Rev.,* **113,** 1458–1469.

Tremback, C. J., 1990: Numerical simulation of a mesoscale convective complex: Model development and numerical results. Ph.D. dissertation, Colorado State University, 247 pp. [Available from University Microfilms, Ann Arbor, MI 48106.]

——, and R. Kessler, 1985: A surface temperature and moisture parameterization for use in mesoscale numerical models. Preprints, *Seventh Conf. on Numerical Weather Prediction,* Montreal, Canada, Amer. Meteor. Soc., 17–20.

Tripoli, G. J., and W. R. Cotton, 1989a: A numerical study of an observed orogenic mesoscale convective system. Part I: Simulated genesis and comparison with observations. *Mon. Wea. Rev.,* **117,** 273–304.

——, and ——, 1989b: A numerical study of an observed orogenic mesoscale convective system. Part II: Analysis of governing dynamics. *Mon. Wea. Rev.,* **117,** 305–328.

Tyson, P. D., and R. A. Preston-Whyte, 1972: Observations of regional topographically-induced wind systems in Natal. *J. Appl. Meteor.,* **11,** 643–650.

Wagner, A., 1938: Theorie und Beobachtung der periodischen Gebirgswinde. *Gerlands Beitr. Geophys.,* **52,** 408–449. [English translation: Whiteman, C. D. and E. Dreiseitl, 1984: Alpine Meteorology. Translations of classic contributions by A. Wagner, E. Ekhart and F. Defant. PNL-5141/ASCOT-84-3. Pacific Northwest Laboratory, Richland, WA, 121 pp.]

Whiteman, C. D., 1980: Breakup of temperature inversions in Colorado mountain valleys. Ph.D. dissertation, Colorado State University, 250 pp. [Available from University Microfilms, Ann Arbor, MI 48106.]